Quantum Property Learning for NISQ Networks: Universal Quantum Witness Machines

Uman Khalid, Junaid ur Rehman, Haejoon Jung, *Senior Member, IEEE*, Trung Q. Duong, *Fellow, IEEE*, Octavia A. Dobre, *Fellow, IEEE*, and Hyundong Shin, *Fellow, IEEE*

***Abstract*—The learning of fundamental quantum properties—namely coherence, discord, and entanglement—benchmarks the security, computational, and metrological capability of noisy intermediate-scale quantum (NISQ) communication, computing, and sensing networks. The current learning techniques vary widely for these fundamental quantum properties, including standard tomographic procedures that involve exhaustive optimization. Fortunately, the fundamentally distinct quantum properties feature an intricate connection. In this paper, we put forth the concept of universal quantum witness machines (UQWMs) to develop a unified framework for quantum property learning (QPL) of a quantum system. We first formulate the certification and quantification of quantum properties based on quantum witnesses. The witness-based certification method is experimentally accessible and resource-efficient but lacks reliability and generality. To universalize the scope and circumvent the unreliability, we transform the certification task into a classification task by employing UQWMs with classical machine learning to construct quantum property classifiers. This formalism offers a unifying perspective on the certification, quantification, and classification of these enigmatically linked fundamental quantum properties. To demonstrate our UQWM approach, we provide a comparative numerical analysis of quantum property quantification with quantum witnesses and classification performance analysis of quantum property classification with convolutional neural networks, specifically for 4×4 quantum systems.**

***Index Terms*—NISQ networks, neural networks, quantum property learning, quantum witness machines.**

I. Introduction

EFFICIENT and reliable characterization of intrinsic quantum properties of unknown quantum systems is a prelude to the development of application-specific near-term quantum networks, e.g., noisy intermediate-scale quantum (NISQ) networks [1]–[3]. The accurate prediction of these properties involves resource-intensive learning procedures [4], [5]. Traditional methods include matrix product state tomography [6], neural network based tomography [7]–[9], and shadow tomography [10]–[12]. First and foremost, among all quantum properties, fundamental quantum properties, namely coherence, discord, and entanglement, lie at the core of developing quantum communication, computing, and sensing technologies ranging from theoretical aspects to practical implementation of their security-incorporated versions [13]–[18].

A. Motivations and Related Work

The transition from classical to quantum networks is attributed to the characterization of quantum properties [19], [20]. The detection criteria of fundamental quantum properties serve as quality metrics to asses and benchmark the performance of quantum networks [21]. These metrics also pose as key signatures of quantum advantage in numerous quantum information processing tasks realizable over NISQ networks [22]. For instance, in case of quantum metrology tasks performed over quantum sensing networks, coherence controls the quantum speed limit of unitary evolution for interferometric phase encoding [23], discord captures the minimal prerequisites for nonzero precision of interferometric phase estimation [24], and entanglement is crucial for surpassing the classical shot-noise limited interferometric phase uncertainty [25]. Similarly, in quantum cryptography tasks over quantum communication networks, coherence operationally quantifies the secret key rate of quantum key distribution protocols [26], discord encapsulates the minimal cryptographic resource requirements [27], and entanglement is critical in extending the scope of quantum key distribution protocols across multipartite systems (i.e., quantum conference key agreement) [28]. This underlines the necessity of discerning resourceful quantum states from resourceless (free) quantum states on account of application-specific advantages.

The quantification of fundamental quantum properties for mixed states is computationally intractable [29]–[31]. Alternately, the trade-off between operational meaning and computational accessibility poses an additional challenge in quantification tasks. In this respect, most noteworthy proposals include quantification of entanglement and coherence by employing their corresponding witnesses [32]–[37]. The witness-based quantifiers establish a lower bound on the corresponding quantum property. However, this research direction still requires significant contributions toward discord quantification.

The fundamental quantum properties are interconvertible and tradeable resources in various quantum information processing experiments [38]. For example, in one-qubit deterministic quantum computation (DQC) experiments, coherence can

This work was supported by a grant from Kyung Hee University in 2023 (KHU-20233663). An earlier version of this paper was presented in part at the 2024 International Conference on Quantum Communications, Networking, and Computing (QCNC). *(Corresponding author: Hyundong Shin.)*

U. Khalid, H. Jung, and H. Shin are with the Department of Electronics and Information Convergence Engineering, Kyung Hee University, 1732 Deogyeong-daero, Giheung-gu, Yongin-si, Gyeonggi-do 17104 Korea (e-mail: hshin@khu.ac.kr).

J. ur Rehman is with is with the Interdisciplinary Centre for Security, Reliability, and Trust (SnT), University of Luxembourg, L-1855, Luxembourg.

T. Q. Duong is with the Faculty of Engineering and Applied Science, Memorial University of Newfoundland, St. John's, NL A1C 5S7, Canada, and is also with the School of Electronics, Electrical Engineering and Computer Science, Queen's University Belfast, Belfast, U.K.

O. A. Dobre is with Department of Electrical and Computer Engineering, Memorial University, 240 Prince Philip Dr., St. John's, NL A1B 3X5 Canada (e-mail: odobre@mun.ca).

be transformed into either discord or entanglement, and vice versa [39], [40]. Moreover, this intricate connection impels operational equivalence and hierarchical relationship among bonafide quantifiers of fundamental quantum properties [41], [42]. This interplay among the enigmatically linked quantum properties urges the necessity for relevant and accurate resource characterization.

Recently, quantum state classification has emerged as a reliable method for detecting quantum properties by utilizing either machine learning (ML) or quantum ML (QML) [43]–[46]. Although the QML algorithms have the potential to offer advantages over ML in certain tasks [47], the classical ML methods are still relatively more mature, scalable, and robust due to the current NISQ technological limitations [48]. Therefore, this research field aims to transform entanglement witness inequalities into reliable classifiers for entangled and separable states using (un)supervised and deep learning techniques [7], [49]–[51]. However, this research avenue is still nascent, with limited contributions regarding ML-based coherence and discord detection.

A unified framework for quantum property learning (QPL) provides a single solution that encompasses all of the aforementioned desirable features [52]. Apart from desirable features of application-specificity, resource relevance, computational efficiency, and scalability towards high dimensionality, this state-of-the-art mechanism should simultaneously cater for intricately linked quantum properties [42], [53]–[55]. Such a unified mechanism outclasses typical QPL methods based on full-state tomography in terms of resource efficiency, post-processing complexity, and time consumption for quantum resource certification and classification [43], [56]–[59]. The benchmark happens as quantum witnesses employ a single compact operator to detect intrinsic properties instead of applying a series of measurements to fully reconstruct the quantum state [60]. Once such witnesses are formulated for quantum property detectors, the respective quantum property quantifiers do not require extra experimental resources [61], [62]. Subsequently, the witness operators in use can be further factored into physical observables, leading to the experimental feasibility [63].

B. Contributions

In this paper, we propose a unified framework to detect fundamental quantum properties, namely coherence, discord, and entanglement. Specifically, we introduce a universal quantum witness machine (UQWM) that employs *witness* measurements and *machine* intelligence. First, we formulate quantum property witness (QPW) inequalities for certification. Then, a finite collection of expectation values of fundamental property witnesses are processed to estimate the fundamental quantum properties. These results are corroborated by comparing these numerically estimated quantifiers with preexisting bonafide quantifiers for some families of test states in the presence of systematic and statistical uncertainties. The proposed UQWM approach is adaptable to incorporate ML and, in turn, serves as a primitive for quantum state classification. To generalize the scope of quantum property certification using the QPW inequalities, we encode expectation values of witness measurements into convolutional neural networks (CNNs) to construct classifiers for general resourceful and resourceless quantum states (density operators). We also demonstrate the prediction performance of these trained classifiers for general quantum states and toy resource states critical for classically nonexistent tasks such as phase estimation beyond the standard quantum limit, teleportation, and trace estimation of unitary operators using one-qubit DQC.

The aforementioned mechanism is designed to integrate seamlessly and operate continuously within the quantum network, where various quantum nodes constantly interact and exchange quantum information. This makes it essential to continually monitor and characterize the quantum properties of these nodes to ensure optimal network performance. For instance, UQWMs can be utilized during the metrological operations of the quantum sensing networks, thereby providing insights into the coherence, discord, and entanglement of the quantum sensing probe preparations prior to their distribution across the network. Furthermore, in these preparations, the ideal pure quantum states are often degraded by noise typical of NISQ devices and networks, leading to mixed quantum states. However, the mechanism is designed to handle these noisy, mixed states effectively, ensuring accurate characterization of fundamental quantum properties within NISQ networks.

We note in passing that our UQWM results highlight the intricate connection among fundamental quantum properties concerning certification and quantification, as well as establish a fruitful analogy between quantum information engineering and data-driven learning. In addition, the UQWM learning is more relevant than standard full-state estimation in practical scenarios in which (i) mere detection of fundamental quantum properties is a primary objective to certify the near-ideal preparation of known target states, (ii) accurate quantification of fundamental quantum properties is required in experiments with the help of partial knowledge about unknown quantum states, and (iii) reliable prediction regarding resourcefulness of unknown quantum states is desired with limited data at hand, prior to any task regarding quantum communication, quantum computation, and quantum metrology.

II. Quantum Property Learning

To unify detection methods of fundamental quantum properties, we introduce the notion of UQWMs, as demonstrated in Fig. 1. The UQWM formalism utilizes a map-and-measure framework to formulate QPW inequalities for coherence, discord, and entanglement.

A. Map-and-Measure Framework

We can represent a $d \times d$ density operator $\boldsymbol{\rho}$ using the generalized Gell–Mann matrix (GGM) basis as follows [64]:

$$\boldsymbol{\rho} = \frac{1}{d}\boldsymbol{I} + \sum_{1\le i<j\le d} (b_{\mathrm{s},ij}\boldsymbol{\Lambda}_{\mathrm{s},ij} + b_{\mathrm{a},ij}\boldsymbol{\Lambda}_{\mathrm{a},ij}) + \sum_{\ell=1}^{d-1} b_{\mathrm{d},\ell}\boldsymbol{\Lambda}_{\mathrm{d},\ell} \tag{1}$$

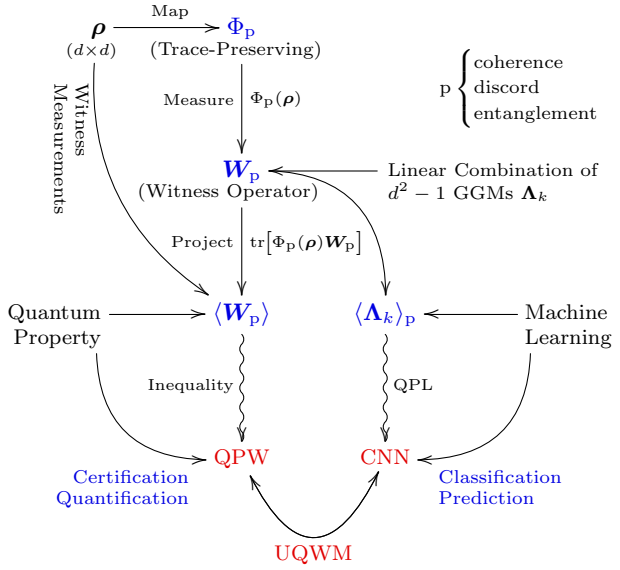

Fig. 1. A diagrammatic illustration for the UQWM formalism. A $d \times d$ density matrix (test quantum state) $\boldsymbol{\rho}$ undergoes a trace-preserving map Φ_{p} and a witness operator $\boldsymbol{W}_{\mathrm{p}}$ in the generalized Gell–Mann matrix basis $\{\boldsymbol{\Lambda}_k\}$ for witness measurements to obtain a linear combination of expectation values $\langle \boldsymbol{\Lambda}_k\rangle_{\mathrm{p}}$ for instantiating the corresponding QPW inequalities. The detection rules established for these inequalities determine whether the test state is resourceful (e.g., coherent, discordant, and entangled) or not. On the one hand, the expectation values $\langle \boldsymbol{\Lambda}_k\rangle_{\mathrm{p}}$ are processed to quantify the corresponding quantum property. On the other hand, these values are fed into CNNs to build quantum property classifiers for resourceful and resourceless states.

with d^2-1 GGMs

$$\begin{cases} \boldsymbol{\Lambda}_{\mathrm{s},ij} = |i\rangle\langle j| + |j\rangle\langle i| \\ \boldsymbol{\Lambda}_{\mathrm{a},ij} = -\iota\,|i\rangle\langle j| + \iota\,|j\rangle\langle i| \\ \boldsymbol{\Lambda}_{\mathrm{d},\ell} = \sqrt{\frac{2}{\ell(\ell+1)}}\left(\sum_{i=1}^{\ell}|i\rangle\langle i| - \ell\,|\ell+1\rangle\langle \ell+1|\right) \end{cases} \tag{2}$$

where $\iota = \sqrt{-1}$; $\boldsymbol{I}$ is the identity operator; $d(d-1)/2$ symmetric $\boldsymbol{\Lambda}_{\mathrm{s},ij}$, $d(d-1)/2$ antisymmetric $\boldsymbol{\Lambda}_{\mathrm{a},ij}$, and $d-1$ diagonal $\boldsymbol{\Lambda}_{\mathrm{d},\ell}$ form a basis for the space of $d \times d$ traceless Hermitian matrices; d^2-1 components $b_{\mathrm{s},ij} = \mathrm{tr}(\boldsymbol{\Lambda}_{\mathrm{s},ij}\boldsymbol{\rho})$, $b_{\mathrm{a},ij} = \mathrm{tr}(\boldsymbol{\Lambda}_{\mathrm{a},ij}\boldsymbol{\rho})$, and $b_{\mathrm{d},\ell} = \mathrm{tr}(\boldsymbol{\Lambda}_{\mathrm{d},\ell}\boldsymbol{\rho})$ form a generalized (d^2-1 dimensional) Bloch vector

$$\begin{aligned}\boldsymbol{b} = \big(&b_{\mathrm{s},12},\ldots,b_{\mathrm{s},(d-1)d}, b_{\mathrm{a},12},\ldots,\\ &b_{\mathrm{a},(d-1)d}, b_{\mathrm{d},1},\ldots,b_{\mathrm{d},d-1}\big)\end{aligned} \tag{3}$$

in a hypersphere of radius

$$\|\boldsymbol{b}\| \leq \delta_d = \sqrt{\frac{d-1}{2d}} \tag{4}$$

and $\mathrm{tr}(\cdot)$ is the trace operator. With the same order in (3), the GGM basis $\{\boldsymbol{\Lambda}_{\mathrm{s},ij}, \boldsymbol{\Lambda}_{\mathrm{a},ij}, \boldsymbol{\Lambda}_{\mathrm{d},\ell}\}$ is denoted by $\{\boldsymbol{\Lambda}_k\}$, $k = 1, 2, \ldots, d^2-1$ for notational simplicity. The test state $\boldsymbol{\rho}$ undergoes a quantum operation described as a trace-preserving map Φ_{p} and is then subject to an experimentally measurable witness operator $\boldsymbol{W}_{\mathrm{p}}$ where the subscript $\mathrm{p} \in \{\mathrm{c}, \mathrm{d}, \mathrm{e}\}$ denotes the relevant quantum property (i.e., coherence, discord, and entanglement) under witness consideration. The optimal construction of witness operators requires optimization routines for fine-tuning involved parameters [30], [32], [54]. Without the loss of generality [33], [56], we employ $d \times d$ Hermitian observables in the weighted GGM basis as witness operators

$$\boldsymbol{W}_{\mathrm{p}} = \sum_{k=0}^{d^2-1} w_{\mathrm{p},k}\boldsymbol{\Lambda}_k \tag{5}$$

ushering random rotations of basis observables with regards to global measurements [65], [66], where $\boldsymbol{\Lambda}_0 = \boldsymbol{I}$ by definition and the witness vector $\boldsymbol{w}_{\mathrm{p}} = \big(w_{\mathrm{p},0}, w_{\mathrm{p},1}, \ldots, w_{\mathrm{p},d^2-1}\big)$ has the weighting components for the GGM basis with $w_k \in [-\delta_d, \delta_d]$. This global measurement projects the mapped test state $\Phi_{\mathrm{p}}(\boldsymbol{\rho})$ to yield the expectation value

$$\langle \boldsymbol{W}_{\mathrm{p}}\rangle = \mathrm{tr}\left[\Phi_{\mathrm{p}}(\boldsymbol{\rho})\,\boldsymbol{W}_{\mathrm{p}}\right], \tag{6}$$

which is a weighted sum of

$$\langle \boldsymbol{\Lambda}_k\rangle_{\mathrm{p}} = \mathrm{tr}\left[\Phi_{\mathrm{p}}(\boldsymbol{\rho})\,\boldsymbol{\Lambda}_k\right]. \tag{7}$$

In most situations, only d values of $\langle \boldsymbol{\Lambda}_k\rangle_{\mathrm{p}}$ are sufficient, instead of all $\langle \boldsymbol{\Lambda}_1\rangle_{\mathrm{p}}, \langle \boldsymbol{\Lambda}_2\rangle_{\mathrm{p}}, \ldots \langle \boldsymbol{\Lambda}_{d^2-1}\rangle_{\mathrm{p}}$, to evaluate many properties of unknown quantum states up to certain precision [67]. Hence, these fundamental properties are evaluated as functions of the expectation values $\langle \boldsymbol{\Lambda}_k\rangle_{\mathrm{p}}$ associated with a set of observables $\{\boldsymbol{\Lambda}_k\}$ for the mapped test state $\Phi_{\mathrm{p}}(\boldsymbol{\rho})$. These functions produce real values that depend on the presence of relevant quantum properties in the test state, enabling the construction of the corresponding QPW inequalities. The detection rules obtained from these inequalities certify inherent quantum property.

Standard approaches for witnessing fundamental quantum properties mainly depend on their chosen witness measurement settings [54], [55], [68]. Moreover, quantifying these properties experimentally with repetitive witness measurements on multiple preparations of a known target state is resource-intensive for several reasons: i) witness measurements often require multiple operations and measurements for accurate property determination; ii) preparing target states repeatedly is challenging and time-consuming; and iii) accurate quantification requires a large number of state preparations. All these put demands on high precision and quality for both the measurement apparatus and target states, leading to the requirement of significant resources. To tackle these challenges, the map-and-measure framework aims to design witness measurements and trace-preserving maps to form a lower bound on the observable fundamental quantum properties. This resource-efficient approach enables quantum property certification for specific classes of test states without extensive device modifications. The detection criteria are then generalized to arbitrary test states by transforming witness inequalities into a classifier with supervised learning.

However, witness-based formalism is susceptible to systematic misalignment errors caused by the imperfect alignment of measurement bases due to the limited device controllability [44], [69], [70]. To demonstrate the error robustness of the map-and-measure framework, we also consider misaligned measurement bases. Note that this framework is compatible with NISQ circuit-level experiments, facilitated by changing the GGM basis to the local Pauli (computational) basis and

decomposing trace-preverving maps in the form of local Pauli basis [64], [71], [72]. In the following, we formulate the certification and quantification of fundamental quantum properties in conjunction with their corresponding witness inequalities.

B. Coherence Witness

Quantum coherence—a key element of fundamental quantum properties—exists even in single-partite systems [52]. Coherence refers to the property of a quantum system wherein a quantum state can exist in a superposition of multiple states simultaneously. The superposition is an elementary feature of quantum mechanics, distinguishing it from classical mechanics and its detection plays a crucial role in quantum biology, quantum thermodynamics, and quantum algorithms [14].

1) Coherence Certification: To detect coherence in an unknown state, the first step involves identifying the corresponding witness operators. For test states, coherence witness operators are traceless Hermitian operators as a linear combination of symmetric and antisymmetric GGMs, given by [73]

$$\boldsymbol{W}_{\mathrm{c}} = \sum_{k=1}^{d(d-1)} w_{\mathrm{c},k} \boldsymbol{\Lambda}_k \tag{8}$$

where the vector $\boldsymbol{w}_{\mathrm{c}} = \big(0, w_{\mathrm{c},1}, w_{\mathrm{c},2}, \ldots, w_{\mathrm{c},d(d-1)}, 0, \ldots, 0\big)$ satisfies the normalization condition $\|\boldsymbol{w}_{\mathrm{c}}\| = \delta_d$; and the first component for the identity operator and the last $d-1$ witness components for the diagonal GGMs are set to zero, i.e.,

$$w_{\mathrm{c},0} = w_{\mathrm{c},d(d-1)+1} = \cdots = w_{\mathrm{c},d^2-1} = 0. \tag{9}$$

Herein, Φ_{c} denotes an incoherent unitary completely positive trace-preserving (CPTP) map. Using a set of Kraus operators $\{\boldsymbol{K}_i\}$, the map Φ_{c} can be written in the operator-sum representation as $\Phi_{\mathrm{c}}(\boldsymbol{\rho}) = \sum_i \boldsymbol{K}_i \boldsymbol{\rho} \boldsymbol{K}_i^{\dagger}$, where the superscript $\dagger$ denotes the transpose conjugate and $\sum_i \boldsymbol{K}_i^{\dagger} \boldsymbol{K}_i = \boldsymbol{I}$. Note that if $\boldsymbol{\rho}$ is an incoherent state, then $\boldsymbol{K}_i \boldsymbol{\rho} \boldsymbol{K}_i^{\dagger}$ is again incoherent, i.e., $\boldsymbol{K}_i \boldsymbol{\rho} \boldsymbol{K}_i^{\dagger} / \operatorname{tr}\big(\boldsymbol{K}_i \boldsymbol{\rho} \boldsymbol{K}_i^{\dagger}\big) \in \mathcal{I}$ for all $\boldsymbol{\rho} \in \mathcal{I}$ where $\mathcal{I}$ is the set of all incoherent states. The coherence detection criterion is presented using the quantum coherence witness inequality

$$\langle \boldsymbol{W}_{\mathrm{c}} \rangle = \operatorname{tr}\left[\Phi_{\mathrm{c}}(\boldsymbol{\rho}) \boldsymbol{W}_{\mathrm{c}}\right] \neq 0 \tag{10}$$

for coherent states where equality is attained only for incoherent states.

Any nonzero expectation $\langle \boldsymbol{\Lambda}_k \rangle_{\mathrm{c}} = \operatorname{tr}\left[\Phi_{\mathrm{c}}(\boldsymbol{\rho}) \boldsymbol{\Lambda}_k\right]$ manifests coherence. Therefore, at least one measurement is necessary to detect coherence; however, detection accuracy can be further enhanced by incorporating all $d(d-1)$ expectation values $\langle \boldsymbol{\Lambda}_k \rangle_{\mathrm{c}}$. Hence, the arbitrary selection of witness coefficients offers a partial solution to the coherence certification problem. This approach outclasses standard tomography where all d^2 observables are critical for detecting coherence in an unknown state after reconstructing the $d \times d$ density matrix.

2) Coherence Quantification: To quantify coherence, we define a measure of coherence in the test state $\boldsymbol{\rho}$ as follows:

$$C(\boldsymbol{\rho}) = \min_{\Phi_{\mathrm{c}}} \sup_{\boldsymbol{W}_{\mathrm{c}}} \operatorname{tr}\left[\Phi_{\mathrm{c}}(\boldsymbol{\rho}) \boldsymbol{W}_{\mathrm{c}}\right]. \tag{11}$$

This measure is suitable for experimental scenarios with no prior knowledge about test states [55] and also forms a lower bound on the observable coherence since $C(\boldsymbol{\rho}) \leq |\operatorname{tr}(\boldsymbol{\rho} \boldsymbol{W}_{\mathrm{c}})|$. In ideal scenarios, the maximum value of $C(\boldsymbol{\rho})$ is achieved for maximally coherent states with their optimal solutions to the witness operator $\boldsymbol{W}_{\mathrm{c}}^{\star}$ (or equivalently $\boldsymbol{w}_{\mathrm{c}}^{\star}$) and the CPTP map $\Phi_{\mathrm{c}}^{\star}$. However, misaligned bases ($\boldsymbol{w}_{\mathrm{c}} \neq \boldsymbol{w}_{\mathrm{c}}^{\star}$) change the chosen witness map ($\Phi_{\mathrm{c}} \neq \Phi_{\mathrm{c}}^{\star}$) and induce systematic errors in coherence quantification. From resource theory of coherence, the measure $C(\boldsymbol{\rho})$ is a bonafide quantifier of coherence: (i) $C(\boldsymbol{\rho}) \geq 0$ with equality if and only if $\boldsymbol{\rho} \in \mathcal{I}$; and (ii) $C(\boldsymbol{\rho}) \geq C(\mathcal{N}(\boldsymbol{\rho}))$, i.e., nonincreasing under any noisy channel $\mathcal{N}$.

3) Numerical Examples: To illustrate the map-and-measure framework for witness estimation of quantum properties, we evaluate general $d \times d$ Haar random density matrices (RDMs) of arbitrary rank r and maximally resourceful mixed states for numerical examples. We specifically investigate the proposed method in terms of resourceful state characterization, framework validity, and inherent errors in estimating fundamental quantum properties.

Purity is also an elementary property of quantum systems as a measure of the degree to which a quantum state is pure or mixed in quantum information processing [74]. The purity of the $d \times d$ density matrix $\boldsymbol{\rho}$ is defined as

$$P(\boldsymbol{\rho}) = \operatorname{tr}\left(\boldsymbol{\rho}^2\right), \tag{12}$$

which ranges from $1/d$ (maximally mixed) to 1 (pure). Geometrically, it is hierarchically related to fundamental quantum properties with the inequality as follows [75]:

$$P(\boldsymbol{\rho}) \geq C(\boldsymbol{\rho}) \geq D(\boldsymbol{\rho}) \geq E(\boldsymbol{\rho}) \tag{13}$$

where $D(\boldsymbol{\rho})$ and $E(\boldsymbol{\rho})$ are discord and entanglement measures given in (18) and (25), respectively. The purity $P(\boldsymbol{\rho})$ also accounts for channel effects that cause the decay of resourceful properties, leading to a figure of merit for characterizing properties in test states. We further verify the developed witness by comparing the estimated values of the formulated measures with preexisting bonafide measures of fundamental quantum properties.

To deal with systematic errors, we incorporate miscalibration in the intended measurement bases by rotating witness bases using $\exp(-\iota\epsilon\boldsymbol{\Lambda}_1)$, while preserving the orthogonality. The rotated GGM basis introduces errors that lead to falsely detecting resource-free states as resourceful or vice versa. It has been observed that quantum states exhibiting greater violations of witness inequalities are more susceptible to statistical errors, while quantum states close to the detection boundary are more likely to be affected by systematic errors [69], [76]. Therefore, we evaluate these errors for a family of test states that exhibit maximal witness violations and transitions from resource-free to resourceful regions.

For coherence estimation, we consider the witness map

$$\Phi_{\mathrm{c}}(\boldsymbol{\rho}) = \boldsymbol{U} \boldsymbol{\rho} \boldsymbol{U}^{\dagger} \tag{14}$$

where $\boldsymbol{U} = \sum_j e^{\iota\phi_j} |j\rangle\langle j|$ is an incoherent unitary operator with parameters $\phi_j \in [0, \pi]$. To optimize the coherence witness map Φ_{c} and operator $\boldsymbol{W}_{\mathrm{c}}$ in (11), we choose at random 100 incoherent unitary operators $\boldsymbol{U}$ and 1000 witness operators $\boldsymbol{W}_{\mathrm{c}}$ for each $\boldsymbol{U}$ using uniformly distributed incoherent parameters ϕ_j and normally distributed witness vectors $\boldsymbol{w}_{\mathrm{c}}$. Hence,

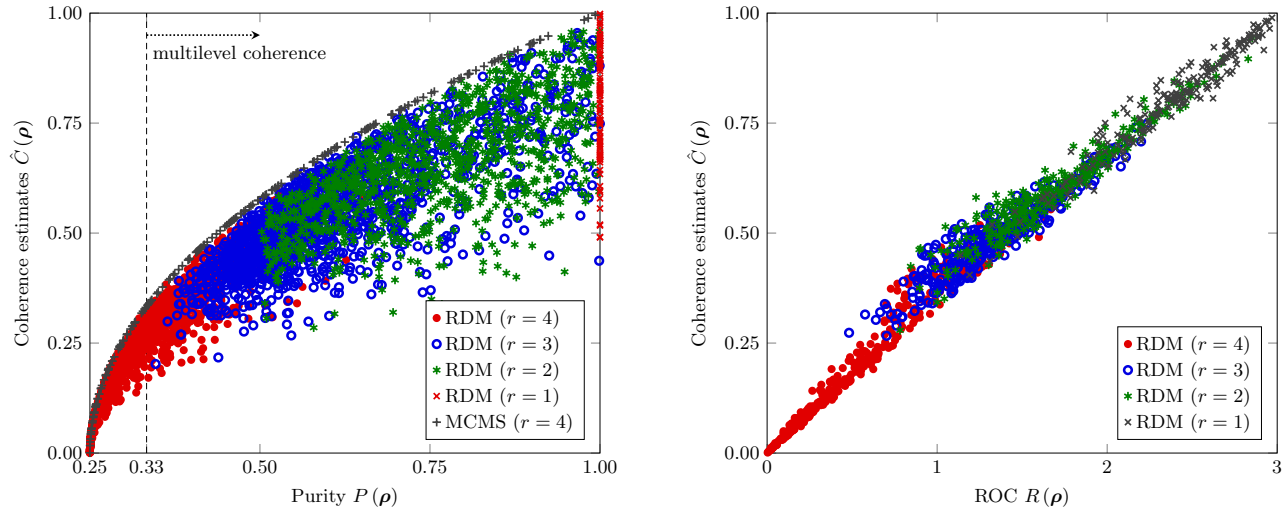

(a) Coherence characterization

(b) Coherence witness validation

Fig. 2. Coherence witness estimation $\hat{C}(\boldsymbol{\rho})$ for RDMs of rank $r=1,2,3,4$ and MCMSs with full rank ($r=4$) when $d=4$. (a) Coherence characterization where coherence estimates $\hat{C}(\boldsymbol{\rho})$ for test states $\boldsymbol{\rho}$ are compared with their purity $P(\boldsymbol{\rho})$. The left and right regions of the dashed line indicate the absence and presence of multilevel coherence. (b) Coherence witness validation where coherence estimates $\hat{C}(\boldsymbol{\rho})$ for RDMs $\boldsymbol{\rho}$ are compared with their ROC $R(\boldsymbol{\rho})$.

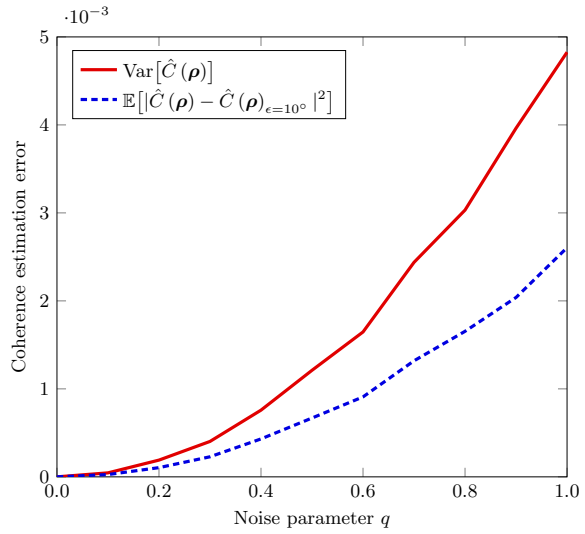

Fig. 3. Statistical and misalignment coherence estimation errors for MCMSs with full rank when $d=4$ where the variance and 10°-misalignment MSE of coherence estimates $\hat{C}(\boldsymbol{\rho})$ are depicted as a function of q, which are obtained by averaging over 1000 trials.

we use 10^5 quantum operations to estimate the coherence measure $C(\boldsymbol{\rho})$ for each test state $\boldsymbol{\rho}$. Herein, each test state $\boldsymbol{\rho}$ refers to a 4×4 quantum system. However, the number of required quantum operations increases significantly with increasing complexity, i.e., the number of subsystems as well as the dimensions of underlying subsystems for noisy quantum systems. As the complexity of such test states grows, the state space expands exponentially, requiring more samples to accurately characterize and optimize the coherence witness. Additionally, quantum noise introduces errors that demand more operations to distinguish coherent from incoherent states and ensure reliable results. Thus, for larger and noisier systems, the required computational and operational resources will increase, potentially making the optimization process more demanding and time-consuming. In such scenarios, alternative optimization approaches besides randomly selecting parameters can be employed. One such approach is gradient-free optimization, where the outputs of the coherence witness function with respect to the parameters are computed to guide the optimization process more efficiently toward the optimal parameters. Evolutionary algorithms, which iteratively improve a population of solutions, can also be used to optimize the coherence witness map and operator more effectively. These methods, by providing more directed and potentially faster convergence to optimal solutions, can offer significant improvements over the currently employed random parameter selection approach.

Note that the coherence measure vanishes only for incoherent states $\boldsymbol{\rho}=\sum_j \lambda_j |j\rangle\langle j|$ where $\sum_j \lambda_j = 1$, while maximally coherent mixed states (MCMSs) form an upper bound on the observable coherence values for test states. For coherence estimation, we also consider a family of MCMSs with full rank decohered under global depolarizing noise with strength $q\in[0,1]$ as follows [77]:

$$\boldsymbol{\rho} = q\,|\psi\rangle\langle\psi| + \frac{1-q}{d}\boldsymbol{I}, \tag{15}$$

which is incoherent for $q=0$, where $|\psi\rangle=\frac{1}{\sqrt{d}}\sum_j |j\rangle$ is the maximally coherent pure state.

Fig. 2 shows coherence witness estimation $\hat{C}(\boldsymbol{\rho})$ for RDMs of rank $r=1,2,3,4$ and MCMSs of full rank ($r=4$) when $d=4$ with its comparison to the purity and an existing bonafide measure of coherence—namely, the robustness of coherence (ROC) [54]. Fig. 2(a) depicts the coherence estimates $\hat{C}(\boldsymbol{\rho})$ and the purity values for test states. We can observe the quantitative relations $P(\boldsymbol{\rho})\geq C(\boldsymbol{\rho})$ and $P(\boldsymbol{\rho})\geq 1/r$ from this test. A higher purity value implies a higher degree

of coherence, while a lower purity value indicates a more mixed state with less coherence. Moreover, the purity also signatures the presence of multilevel coherence for states satisfying $P(\boldsymbol{\rho}) > 1/(d-1)$ [33]. To validate the nullity, Fig. 2(b) compares coherence estimates $\hat{C}(\boldsymbol{\rho})$ with the ROC, ensuring that there is no anomaly in the measure and the witness-based detection method is functioning correctly. It is important to note that $\hat{C}(\boldsymbol{\rho})$ does not directly estimate the ROC, as both measures are inherently distinct. Instead, this comparison serves to verify that the employed method aligns with established measures in specific cases without directly quantifying them, thereby ensuring the reliability and accuracy of witness-based detection. To ascertain the effect of basis misalignment errors, Fig. 3 shows the coherence estimation imprecision for error-prone quantum measurement devices where the variance $\mathrm{Var}[\hat{C}(\boldsymbol{\rho})]$ and 10°-misalignment mean squared error (MSE) $\mathbb{E}[|\hat{C}(\boldsymbol{\rho}) - \hat{C}(\boldsymbol{\rho})_{\epsilon=10^\circ}|^2]$ of coherence estimates $\hat{C}(\boldsymbol{\rho})$ for MCMS $\boldsymbol{\rho}$ in (15) are depicted as a function of q. We can observe the limited imprecision in the coherence estimation from these statistical and misalignment error scales.

C. Discord Witness

Quantum discord—the most general form of fundamental quantum properties—operationally coincides with basis-free coherence for separable states at a minimum and entanglement for pure entangled states at a maximum [42]. Discord refers to the non-classical correlations present between subsystems of a quantum system, thereby capturing a broader range of quantum correlations that can exist even in separable states. It highlights the presence of quantum effects that cannot be fully explained by classical information theory. Unfortunately, it is infeasible to detect quantum discord in separable states with linear witness operators despite its detection being closely related to phenomena such as remote state preparation, quantum phase transitions, and quantum channel discrimination [15].

1) Discord Certification: Despite some useful relations between coherence and discord in some cases, coherence is a basis-dependent quantity, in contrast to discord. However, by leveraging the equivalence between basis-free coherence and discord in multipartite states, we provide a feasible detection criterion for witnessing symmetric discord of unknown states. Therefore, in the UQWM formalism, coherence and discord are treated independently, as the witness operators are designed to certify their respective quantum properties. For test states, discord witness operators are traceless Hermitian operators again as a linear combination of symmetric and antisymmetric GGMs:

$$\boldsymbol{W}_{\mathrm{d}} = \sum_{k=1}^{d(d-1)} w_{\mathrm{d},k} \boldsymbol{\Lambda}_k \tag{16}$$

where $\boldsymbol{w}_{\mathrm{d}} = \big(0, w_{\mathrm{d},1}, w_{\mathrm{d},2}, \ldots, w_{\mathrm{d},d(d-1)}, 0, \ldots, 0\big)$ satisfies $\|\boldsymbol{w}_{\mathrm{d}}\| \leq \delta_d$. Herein, Φ_{d} is a local incoherent unitary transformation map. Therefore, the detection criterion for symmetric discord is formulated using the discord witness inequality

$$\langle \boldsymbol{W}_{\mathrm{d}} \rangle = \mathrm{tr}\left[\Phi_{\mathrm{d}}(\boldsymbol{\rho}) \boldsymbol{W}_{\mathrm{d}}\right] \neq 0 \tag{17}$$

for discordant states, whereas equality is obtained only for completely nondiscordant states.

Any nonzero significant value in $\langle \boldsymbol{\Lambda}_k \rangle_{\mathrm{d}} = \mathrm{tr}\left[\Phi_{\mathrm{d}}(\boldsymbol{\rho}) \boldsymbol{\Lambda}_k\right]$ exhibits the presence of discord. The detection confidence is increased by employing all nonzero values from total $d(d-1)$ expectation values $\langle \boldsymbol{\Lambda}_k \rangle_{\mathrm{d}}$. Therefore, this witnessing method is more computationally efficient than standard tomography. The discord witness inequality (17) implies minimum detectable nonclassical properties, which have direct operational interpretation for quantum information processing tasks undergoing without entanglement.

2) Discord Quantification: In general, discord computation is NP-complete, but we can invoke a discord estimate using

$$D(\boldsymbol{\rho}) = \min_{\Phi_{\mathrm{d}}} \sup_{\boldsymbol{W}_{\mathrm{d}}} \mathrm{tr}\left[\Phi_{\mathrm{d}}(\boldsymbol{\rho}) \boldsymbol{W}_{\mathrm{d}}\right]. \tag{18}$$

Optimistically, the optimal witness vector $\boldsymbol{w}_{\mathrm{d}}^\star$ and CPTP map $\Phi_{\mathrm{d}}^\star$ are aligned such that maximum values of $D(\boldsymbol{\rho})$ are found for maximally discordant test states and the minimum values for nondiscordant test states. However, angular deviations of reference basis change the chosen optimal map $\Phi_{\mathrm{c}}^\star$ and induce systematic errors in discord quantification. With reference to resource theory of discord, the measure $D(\boldsymbol{\rho})$ is a bonafide discord quantifier owing to the properties: (i) $D(\boldsymbol{\rho}) \geq 0$, left discord $D_{\mathrm{L}}(\boldsymbol{\rho}_{\mathrm{AB}}) \geq 0$, and right discord $D_{\mathrm{R}}(\boldsymbol{\rho}_{\mathrm{AB}}) \geq 0$, i.e., nonnegative for all states and nonzero for almost all quantum states; (ii) $D(\boldsymbol{\rho}) \geq D(\mathcal{N}(\boldsymbol{\rho}))$, i.e., nonincreasing under any noisy channel $\mathcal{N}$; and (iii) $D_{\mathrm{L}}(\boldsymbol{\rho}_{\mathrm{AB}}) \neq D_{\mathrm{R}}(\boldsymbol{\rho}_{\mathrm{AB}}) \geq 0$ in general, i.e., asymmetric in left and right discord.

3) Numerical Examples: For discord estimation, we consider the witness map Φ_{d} for a bipartite system as follows:

$$\Phi_{\mathrm{d}}(\boldsymbol{\rho}) = (\boldsymbol{U}_{\mathrm{A}} \otimes \boldsymbol{U}_{\mathrm{B}}) \boldsymbol{\rho} (\boldsymbol{U}_{\mathrm{A}} \otimes \boldsymbol{U}_{\mathrm{B}})^\dagger \tag{19}$$

where $\boldsymbol{U}_{\mathrm{A}}$ and $\boldsymbol{U}_{\mathrm{B}}$ are local unitary operators; and $\otimes$ denotes the tensor product. Note that the discord measure $D(\boldsymbol{\rho})$ for this bipartite system acts as an estimate for symmetric discord that is the average of left and right discord values—$D_{\mathrm{L}}(\boldsymbol{\rho})$ and $D_{\mathrm{R}}(\boldsymbol{\rho})$—and vanishes only for left- and right-nondiscordant states $\boldsymbol{\rho} = \sum_j \lambda_j |j\rangle\langle j| \otimes |j\rangle\langle j|$ where $\sum_j \lambda_j = 1$. For discord estimation, we also consider a family of MDMSs for $d = 4$:

$$\boldsymbol{\rho} = q |\mathsf{bell}\rangle\langle \mathsf{bell}| + (1-q)\left(\mu |01\rangle\langle 01| + (1-\mu) |10\rangle\langle 10|\right) \tag{20}$$

where $q, \mu \in [0,1]$ and $|\mathsf{bell}\rangle = \left(|00\rangle + |11\rangle\right)/\sqrt{2}$ is the Bell state [78]. This MDMS exhibits rank 2 for $\mu = 0, 1$ and rank 3 otherwise. For MDMSs with full rank ($r = 4$), we consider

$$\boldsymbol{\rho} = q |\mathsf{bell}\rangle\langle \mathsf{bell}| + \frac{1-q}{d} \boldsymbol{I}. \tag{21}$$

Fig. 4 shows discord witness estimation for $d = 4$. Fig. 4(a) depicts the discord estimates $\hat{D}(\boldsymbol{\rho})$ and the purity values for RDMs of rank $r = 1, 2, 3, 4$ and MDMSs of full rank ($r = 4$). The discord is typically an observer-dependent quantity, i.e., it has its left and right variants based on the measurement side. For completely nondiscordant (classical) states, this discord witnessing is evident. However, its true advantage is revealed when test states possess only one-sided (either left or right) discord. By fixing $\boldsymbol{U}_{\mathrm{A}} = \boldsymbol{I}$ or $\boldsymbol{U}_{\mathrm{B}} = \boldsymbol{I}$,

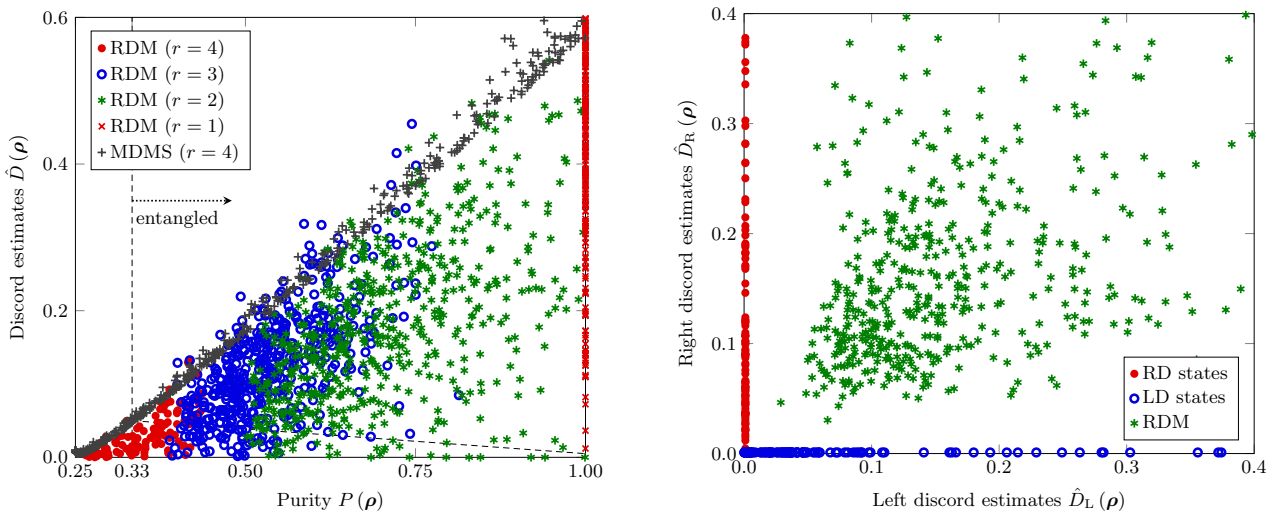

(a) Discord characterization

(b) Discord witness validation

Fig. 4. Discord witness estimation for $d=4$. (a) Discord characterization where discord estimates $\hat{D}(\boldsymbol{\rho})$ for RDMs of rank $r=1,2,3,4$ and MDMSs of full rank ($r=4$) are compared with their purity $P(\boldsymbol{\rho})$. The left and right regions of the dashed line indicate the absence and presence of entanglement. (b) Discord witness validation where left discord estimates $\hat{D}_{\mathrm{L}}(\boldsymbol{\rho})$ are compared with right discord estimates $\hat{D}_{\mathrm{R}}(\boldsymbol{\rho})$ for LD states, RD states, and RDMs of arbitrary rank r to verify the nullity and asymmetry in these one-sided discord values for special families of discordant states.

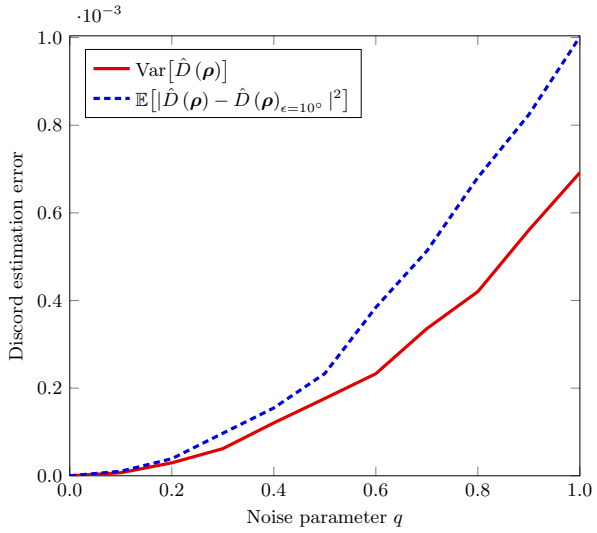

Fig. 5. Statistical and misalignment discord estimation errors for MDMSs with full rank ($r=4$) where the variance and 10°-misalignment MSE of discord estimates $\hat{D}(\boldsymbol{\rho})$ are depicted as a function of q by averaging over 1000 trials.

we can estimate the left $\hat{D}_{\mathrm{L}}(\boldsymbol{\rho})$ or right discord $\hat{D}_{\mathrm{R}}(\boldsymbol{\rho})$ of test states $\boldsymbol{\rho}$ using the proposed discord quantification. Hence, the left and right discord estimates vanish for right-discordant (RD) states $\sum_j \lambda_j |j\rangle\langle j| \otimes \boldsymbol{\rho}_{\mathrm{B},j}$ and left-discordant (LD) states $\sum_j \lambda_j \boldsymbol{\rho}_{\mathrm{A},j} \otimes |j\rangle\langle j|$, respectively. For validation, Fig. 4(b) depicts one-sided discord estimates $\hat{D}_{\mathrm{L}}(\boldsymbol{\rho})$ and $\hat{D}_{\mathrm{R}}(\boldsymbol{\rho})$ for LD states, RD states, and RDMs of arbitrary rank r. This example validates the nullity condition as well as the asymmetric property of the discord measure by comparing left and right discord estimates for these two special classes of discordant states. Fig. 5 shows the discord estimation imprecision where the variance $\mathrm{Var}[\hat{D}(\boldsymbol{\rho})]$ and 10°-misalignment MSE $\mathbb{E}[|\hat{D}(\boldsymbol{\rho})-\hat{D}(\boldsymbol{\rho})_{\epsilon=10^{\circ}}|^2]$ of discord estimates $\hat{D}(\boldsymbol{\rho})$ for full-rank MDMSs ($r=4$) are depicted as a function of q to ascertain the effect of basis misalignment errors in discord estimation.

D. Entanglement Witness

Quantum entanglement—an exclusive property of quantum systems—is vital for establishing the computational advantage of quantum information processors over their classical counterparts [13]. Entanglement refers to the quantum correlations between subsystems of a quantum system, where the state of one subsystem cannot be described independently of the state of other interconnected subsystems. This means that a measurement on one subsystem instantly influences the state of the other subsystems, regardless of their spatial separation.

1) Entanglement Certification: Entanglement witness is the most efficient way to certify entanglement in a quantum state. For test states, entanglement witness operators are given by

$$\boldsymbol{W}_{\mathrm{e}} = \sum_{k=0}^{d^2-1} w_{\mathrm{e},k} \boldsymbol{\Lambda}_k \tag{22}$$

where the witness vector $\boldsymbol{w}_{\mathrm{e}} = \left(1/d, w_{\mathrm{e},1}, w_{\mathrm{e},2}, \ldots, w_{\mathrm{e},d^2-1}\right)$ satisfies $\|\boldsymbol{w}_{\mathrm{e}}\| \leq \sqrt{\delta_d^2 + 1/d^2}$ corresponding to $\mathrm{tr}(\boldsymbol{W}_{\mathrm{e}}) = 1$. The entanglement witness map Φ_{e} is trace-preserving but not completely positive. One way to describe such a map is the operator-sum-difference representation

$$\begin{aligned}\Phi_{\mathrm{e}}(\boldsymbol{\rho}) &= \Phi_{\mathrm{e}}^{+}(\boldsymbol{\rho}) - \Phi_{\mathrm{e}}^{-}(\boldsymbol{\rho}) \\ &= \sum_{\lambda_i>0} \lambda_i \boldsymbol{K}_i \boldsymbol{\rho} \boldsymbol{K}_i^{\dagger} + \sum_{\lambda_i<0} \lambda_i \boldsymbol{K}_i \boldsymbol{\rho} \boldsymbol{K}_i^{\dagger}\end{aligned} \tag{23}$$

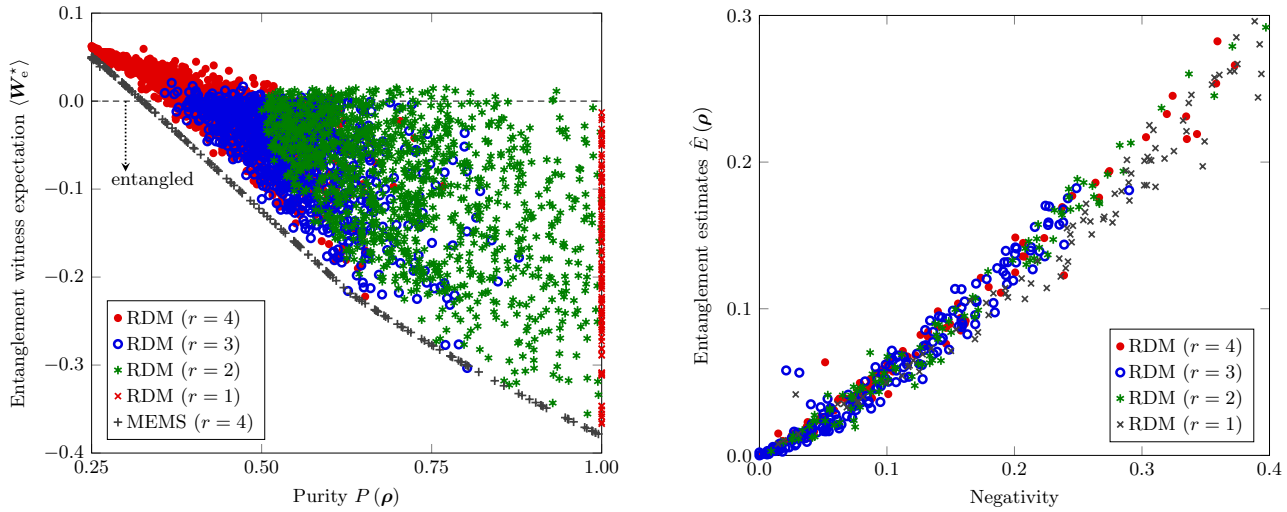

(a) Entanglement characterization

(b) Entanglement witness validation

Fig. 6. Entanglement witness estimation for $d = 4$. (a) Entanglement characterization where the optimal entanglement witness expectation $\langle \boldsymbol{W}_{\mathrm{e}}^{\star} \rangle$ for RDMs of rank $r = 1, 2, 3, 4$ and MEMSs with full rank ($r = 4$) are compared with their purity $P(\boldsymbol{\rho})$ where $\boldsymbol{W}_{\mathrm{e}}^{\star}$ denotes the optimal entanglement witness operator chosen for entanglement estimation $\hat{E}(\boldsymbol{\rho})$. The upper and lower regions of the dashed line indicate the absence and presence of entanglement. (b) Entanglement witness validation where entanglement estimates $\hat{E}(\boldsymbol{\rho})$ for RDMs $\boldsymbol{\rho}$ are compared with their negativity values.

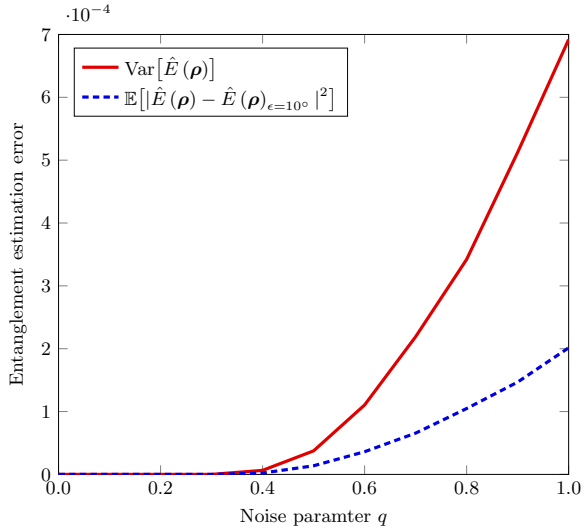

Fig. 7. Statistical and misalignment entanglement estimation errors for MEMSs when $d = 4$ where the variance and 10°-misalignment MSE of entanglement estimates $\hat{E}(\boldsymbol{\rho})$ are depicted as a function of q by averaging over 1000 trials.

where $\Phi_{\mathrm{e}}^{\pm}$ are CPTP maps. For entanglement detection, the entanglement witness inequality is constructed as

$$\langle \boldsymbol{W}_{\mathrm{e}} \rangle = \mathrm{tr}\left[\Phi_{\mathrm{e}}(\boldsymbol{\rho})\, \boldsymbol{W}_{\mathrm{e}}\right] < 0 \tag{24}$$

where inequality is violated only by separable states. The minimum value in $\langle \boldsymbol{W}_{\mathrm{e}} \rangle$ is obtained for the projector $\boldsymbol{P}_{\min}$ corresponding to the minimum eigenvalue $\lambda_{\min}$ in pure decomposition $\Phi_{\mathrm{e}}(\boldsymbol{\rho}) = \sum_j \lambda_j \boldsymbol{P}_j$ such that $\Phi_{\mathrm{e}}(\boldsymbol{\rho})\, \boldsymbol{P}_{\min} = \lambda_{\min} \boldsymbol{P}_{\min}$.

2) Entanglement Quantification: Interestingly, we can also estimate entanglement content in test states using

$$E(\boldsymbol{\rho}) = \max\left\{0, \sup_{\boldsymbol{W}_{\mathrm{e}}} \left(-\mathrm{tr}\left[\Phi_{\mathrm{e}}(\boldsymbol{\rho})\, \boldsymbol{W}_{\mathrm{e}}\right]\right)\right\}. \tag{25}$$

This is in effect an experimentally measurable bonafide quantifier of entanglement due to the fact that: (i) $E(\boldsymbol{\rho}) = 0$ only for separable states; (ii) $E(\boldsymbol{\rho}) \geq \sum_i p_i E(\boldsymbol{\rho}_i)$, i.e., monotonically nonincreasing under local operations and classical communication (LOCC) where $p_i = \mathrm{tr}\left(\boldsymbol{K}_i \boldsymbol{\rho} \boldsymbol{K}_i^{\dagger}\right)$ and $\boldsymbol{\rho}_i = \frac{1}{p_i} \boldsymbol{K}_i \boldsymbol{\rho} \boldsymbol{K}_i^{\dagger}$ with Kraus operators $\boldsymbol{K}_i$; and (iii) $E\left(\boldsymbol{U} \boldsymbol{\rho} \boldsymbol{U}^{\dagger}\right) = E(\boldsymbol{\rho})$, i.e, invariant under local unitary transformation $\boldsymbol{U} = \boldsymbol{U}_{\mathrm{A}} \otimes \boldsymbol{U}_{\mathrm{B}}$.

It follows from Choi-Jamiołkowski isomorphism that the witness observable $\boldsymbol{W}_{\mathrm{e}}$ is also a quantum state in the closest proximity to the test state [79]. This implies that an entangled state may serve as a witness for detecting entanglement. The mean proximity in terms of the mean squared Hilbert-Schmidt distance between the test state $\boldsymbol{\rho}$ and randomly drawn witness operators $\boldsymbol{W}_{\mathrm{e}}$ is upper bounded by $P(\boldsymbol{\rho})$ [80]. In other words, the problem of constructing an optimal entanglement witness using standard optimization techniques transforms into finding a state largely overlapping with the test state in a bounded search space that maximizes $E(\boldsymbol{\rho})$. It in turn confirms the fact that some information about the test state is required in advance to construct a fine optimal witness [63], [68]. This approach appears to be better than fidelity-based entanglement witness methods requiring full knowledge about target states in the sense that it provides a reliable way to optimally measure the entanglement of unknown random states. If little information about test states is available, the entanglement measure $E(\boldsymbol{\rho})$ establishes a lower bound on its intrinsic entanglement. However, misalignment in the GGM basis again causes errors in entanglement estimation.

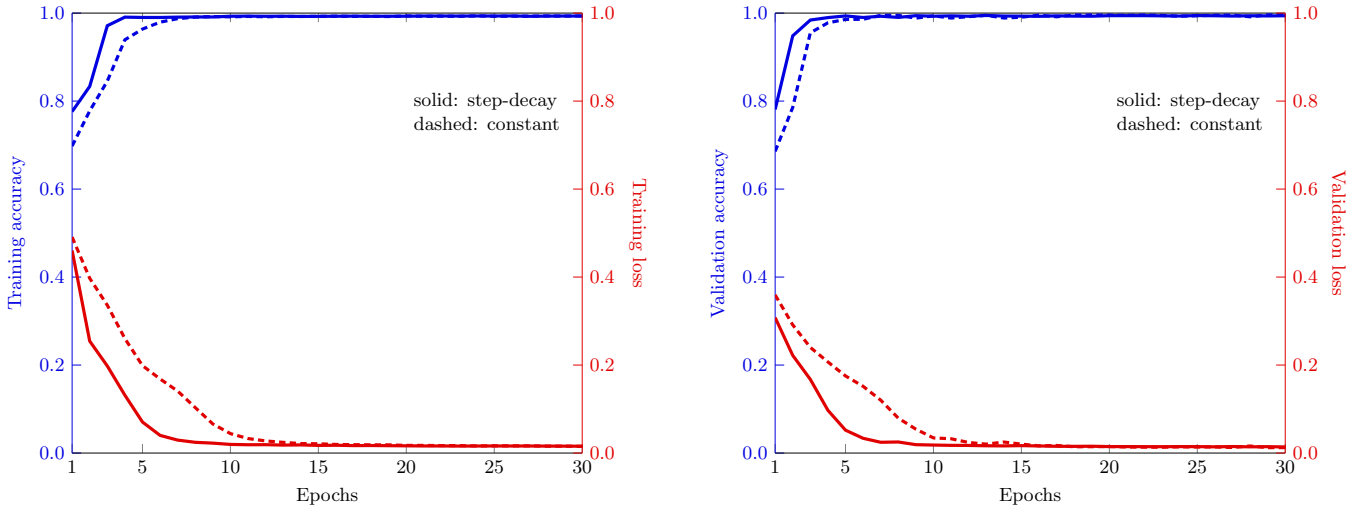

(a) Training (b) Validation

Fig. 8. Coherence classification where (a) training and (b) validation accuracy and loss values are plotted as a function of epochs for the step-decay and constant learning rates.

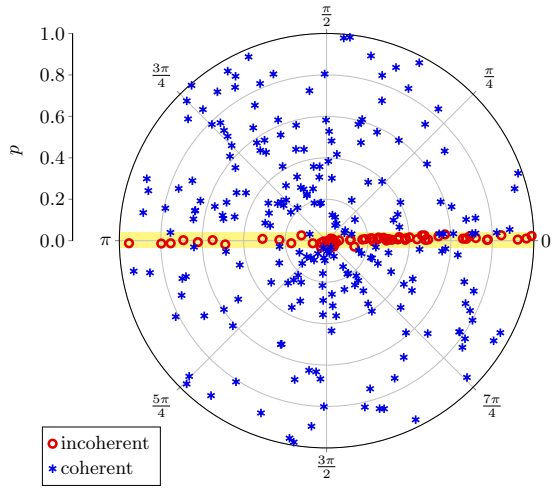

Fig. 9. Toy coherence detection where the prediction results with the trained toy CNN model are depicted as a function of parameters (p, θ) for a toy example of (27) on coherent and incoherent regions. The blue and red data points represent predictions as coherent and incoherent, respectively. The yellow-shaded region depicts the actual incoherent region.

3) Numerical Examples: For entanglement estimation, we consider the reduction witness map Φ_{e} for a bipartite quantum system as follows:

$$\Phi_{\mathrm{e}}(\boldsymbol{\rho}) = \boldsymbol{\rho}_{\mathrm{A}} \otimes \boldsymbol{I} - \boldsymbol{\rho}_{\mathrm{AB}}. \tag{26}$$

The entanglement witness $\langle \boldsymbol{W}_{\mathrm{e}} \rangle$ is nonnegative for a separable RDM $\boldsymbol{\rho} = \sum_j \lambda_j \boldsymbol{\rho}_{\mathrm{A},j} \otimes \boldsymbol{\rho}_{\mathrm{B},j}$ where $\sum_j \lambda_j = 1$, while this expectation exhibits negative values for entangled RDMs. For test states, we also consider a family of maximally entangled mixed states (MEMSs) with full rank in (21) for $d = 4$ where the Bell state $|\mathsf{bell}\rangle$ is a maximally entangled pure state.

Fig. 6 shows entanglement witness estimation for $d = 4$. Fig. 6(a) depicts the optimal entanglement witness expectation $\langle \boldsymbol{W}_{\mathrm{e}}^{\star} \rangle$ and the purity values for RDMs of rank $r = 1, 2, 3, 4$ and MEMSs with full rank ($r = 4$), where $\boldsymbol{W}_{\mathrm{e}}^{\star}$ denotes the optimal entanglement witness operator chosen for entanglement estimation $\hat{E}(\boldsymbol{\rho})$. To ensure the method is functioning correctly, Fig. 6(b) compares the entanglement estimates $\hat{E}(\boldsymbol{\rho})$ with the existing bonafide measure of entanglement—namely, negativity [13]—thereby validating the nullity. Fig. 7 shows the entanglement estimation imprecision where the variance and 10°-misalignment MSE of entanglement estimates $\hat{E}(\boldsymbol{\rho})$ for MEMSs with full rank are depicted as a function of q. We can observe highly reliable entanglement estimation against systematic imprecision and robustness under statistical uncertainty even for MEMSs with a maximal violation of entanglement witness inequality.

III. Neural Networks for QPL

Efficient and reliable classification of quantum states is vital for quantum information processing, despite being computationally burdensome [45], [81]. To this end, we employ (10), (17), and (24) to implement a reliable classifier that categorizes quantum states as either coherent or incoherent, discordant or nondiscordant, and entangled or separable. Moreover, this approach effectively minimizes unreliable detection, predominantly found in witness-based detection methods [46]. In essence, it universalizes the witness-based detection criteria by delimiting its scope from specific test states to arbitrary test states. While witnesses can somewhat accurately estimate coherence, discord, and entanglement for predefined specific state families with some prior knowledge about the underlying test states, ML models can generalize these criteria to classify an arbitrary set of unknown quantum states without requiring tailored witnesses for each specific family. Herein, specific test state families refer to quantum states for which the witnesses are explicitly designed and calibrated, optimizing performance based on known properties and behaviors within this limited set. In contrast, arbitrary test states encompass

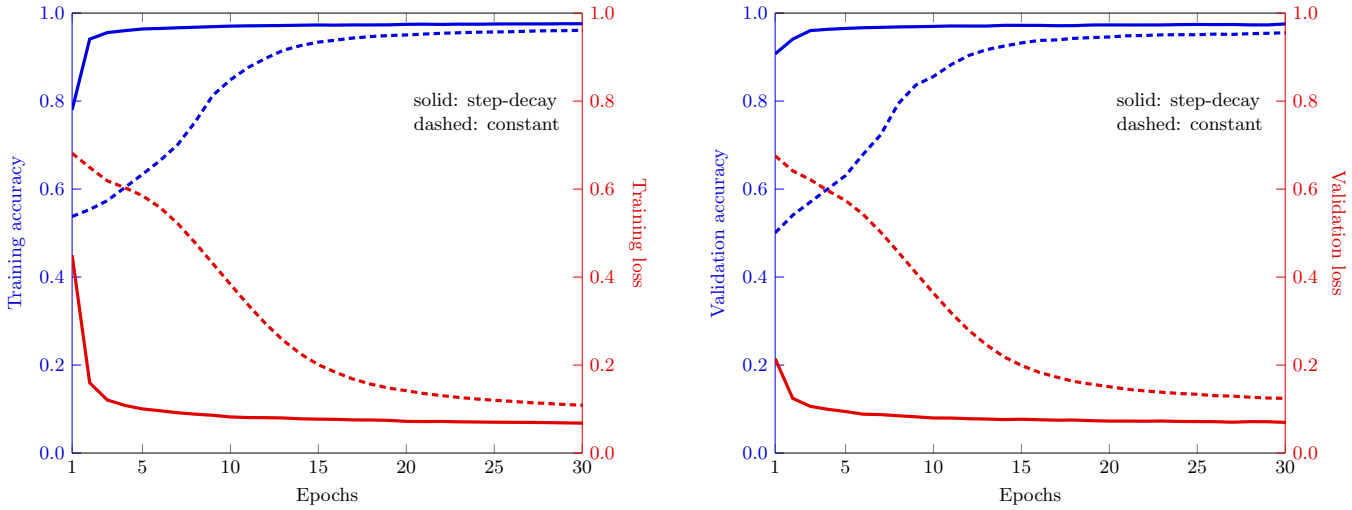

(a) Training (b) Validation

Fig. 10. Discord classification where (a) training and (b) validation accuracy and loss values are plotted as a function of epochs for the step-decay and constant learning rates.

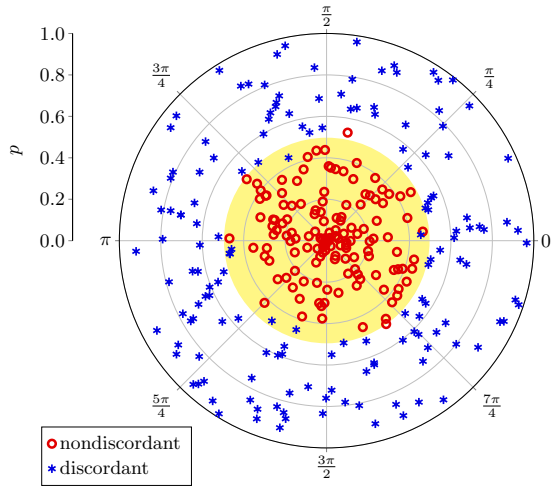

Fig. 11. Toy discord detection where the prediction results with the trained toy CNN model are depicted as a function of parameters (p, θ) for a toy example of (28) on discordant and nondiscordant regions. The blue and red data points represent predictions as discordant and nondiscordant, respectively. The yellow-shaded region depicts the actual nondiscordant region.

TABLE I
CLASSIFICATION REPORTS FOR THE 1D-CNN LENET-5 MODEL WITH THE STEP-DECAY LEARNING RATE.

Class	Precision	Recall	F1-Score	Support
Incoherent	0.98	0.99	0.98	1288
Coherent	1.00	1.00	1.00	4712
Accuracy	N/A	N/A	0.99	6000
Macro Avg	0.99	0.99	0.99	6000
Nondiscordant	0.96	0.97	0.96	5314
Discordant	0.98	0.98	0.98	10686
Accuracy	N/A	N/A	0.98	16000
Macro Avg	0.97	0.97	0.97	16000
Separable	1.00	1.00	1.00	12554
Entangled	1.00	1.00	1.00	17446
Accuracy	N/A	N/A	1.00	30000
Macro Avg	1.00	1.00	1.00	30000

a broader range of quantum states that may not fit into these categories, potentially exhibiting unexpected complex behaviors that specific witnesses might not accurately detect. Therefore, the universal approach enhances the flexibility and applicability of the witness-based detection method, making it robust against variations in the test quantum states. Such binary classifiers can be realized with sufficient measurement data by employing conventional ML techniques. The CNN architecture containing convolutional, pooling, and fully connected layers transforms linear quantum witness inequalities to nonlinear binary quantum state classifiers. The input vector contains expectation values $\langle \mathbf{\Lambda}_k \rangle_{\mathrm{p}}$ for a set of observables associated with the mapped test states. In the supervised learning process, these experimentally extracted measurement data are binary labeled using the reliable detection method of a relevant quantum property. The dataset generated for a large but finite number of test states is fed to a classification model for training and validation. At the testing phase, the test set is subject to making predictions over the validated model to evaluate the classification performance of the model. Finally, this fine-tuned classifier predicts unknown quantum states in view of their application-specific resourcefulness.

A. Architecture and Learning Models

The model architecture is the one-dimensional (1D)-CNN *LeNet-5* which is an effective choice for the 4×4 test states, where the expectation values $\langle \mathbf{\Lambda}_k \rangle_{\mathrm{p}}$ are fed to the input layer. This model has two convolutional layers with each followed by a max-pooling layer, a dropout layer, a flattening layer, and three fully connected layers. All layers are activated using the nonlinear yet faster-to-compute ReLU function, except the output layer, which is activated using the Softmax function.

The output layer is fixed at two neurons for binary classifiers. The output at each neuron corresponds to the probability that a quantum state is either coherent or incoherent, discordant or nondiscordant, and entangled or unentangled. The architecture is implemented using Sequential API in Keras on Tensorflow V2.12.0 while the remaining settings and parameters are kept at default. The simple architecture effectively captures local dependencies and hierarchical structures in the expectation value data in accordance with symmetric, antisymmetric, and diagonal GGM components. The underlying convolutional layers extract relevant features from the input measurement values of mapped quantum states, making the classification process more efficient and accurate by reducing data dimensionality while preserving essential information. While this architecture is well-suited for the specific task of classifying 4×4 quantum states, the optimal ML architecture can vary depending on the specific properties of the quantum systems. For example, artificial neural networks (ANNs) are effective in estimating quantum state fidelity, while two-dimensional (2D)-CNNs are well-suited for multi-class classification of various types of optical quantum states from their corresponding Wigner functions image data [7]. Now, we implement the transformation of linear quantum witnesses of coherence, discord, and entanglement to their binary classifiers and analyze its classification performance for general 4×4 dimensional quantum systems on account of reliability and generality. The quality, diversity, and size of the corresponding master datasets are the main factors in the effective training, validation, and testing of the model's generalization performance. The quality of datasets is maintained through noise-free witness measurements and correct labeling. However, in realistic experimental settings, noisy witness measurements can decrease accuracy, affect robustness, and increase bias and variance in the model, significantly impacting the performance of ML models trained on such noisy data. Fortunately, CNNs can somewhat handle variations and noise in the input data, given the intrinsic noisy quantum systems and misaligned witness measurements. Moreover, the pooling layers in CNNs further enhance this capability by providing translational invariance, ensuring that slight variations in the input expectation value data do not significantly affect the classification performance. The binary data labeling for coherence, discord, and entanglement is achieved using their bonafide quantifiers such as ROC, local quantum uncertainty, and negativity, respectively [13], [54], [82]. The cost of accurate data labeling is eliminated in unsupervised learning cases, but at the expense of classification accuracy and increased size of datasets [50]. To avoid bias, master datasets are generated with approximately equal ratios of coherent and incoherent, discordant and nondiscordant, as well as entangled and separable states. The datasets are formed from a wide variety of underlying resourceful-resourceless quantum states. Such data diversity is faithfully reflected in the ability of classifiers to generalize well to new unseen quantum states. We investigate the CNN performance for QPL in non-toy environments—where the CNN model is trained over master datasets—as well as toy environments—where the CNN model is trained over datasets of only toy samples. As toy examples, we evaluate some notable quantum states central to practical quantum information processing scenarios. The labeled master datasets are divided into training, validation, and testing sets in the ratio $6.4:1.6:2$. The accuracy and loss are employed to evaluate the classification performance of data-driven QPL models during the training, validation, and testing phases. The batch size is set to 128. During model compilation, *sparse categorical cross-entropy* is employed as the loss function and *Adam* as the optimizer with default hyperparameters but varying the learning rate $L_{\rm p}$. We utilize callbacks with early stopping patience set to 10 for monitoring and identifying the best model. In addition, we also incorporate the step-decay learning rate scheduling for fast convergence and a dropout regularization layer (with a fraction of 0.25) before flattening the layer to prevent overfitting to the training data.

B. Coherence Classification

1) Dataset Formulation: The master dataset for coherence is comprised of total $30,000$ instances. This dataset contains $10,000$ samples of RDMs with arbitrary rank r, $10,000$ samples of pure RDMs ($r = 1$) decohered under global depolarizing noise, and $10,000$ samples of RDMs with full rank ($r = 4$) strongly decohered under global depolarizing noise with noise parameter values $q < 0.1$. All these density matrices are generated, mapped, measured, and labeled using functions available in the QETLAB package, a MATLAB toolbox for exploring quantum entanglement theory.

2) Numerical Results: Fig. 8(a) shows the trainability of the CNN model in quantum coherence learning where the training accuracy and loss rapidly converge to 99.401% and 1.466% for the step-decay learning rate (initialized at 0.0002) and 99.381% and 1.299% for the constant learning rate of $L_{\rm c} = 0.0001$. Fig. 8(b) validates the trained model where the validation accuracy and loss are 99.395% (99.166%) and 1.355% (1.336%) for the step-decay (constant) learning rate for new and unseen coherent or incoherent data instances. For this trained model, the testing accuracy and loss are 99.283% and 1.525% for the step-decay learning rate and 99.279% and 1.628% for the constant learning rate. The classification reports for the trained LeNet-5 model with the step-decay learning rate are detailed in Table I.

3) Toy Coherence Detection: For a toy example, we evaluate a coherence detector for the following coherent mixed state marking the quantum advantage in a phase discrimination task:

$$\boldsymbol{\rho} = p\,|\mathsf{toy}_{\rm c}\rangle\langle\mathsf{toy}_{\rm c}| + \frac{(1-p)\,\boldsymbol{I}}{d} \tag{27}$$

where $|\mathsf{toy}_{\rm c}\rangle = \cos(\theta/2)\,|0\rangle + e^{\iota\phi}\sin(\theta/2)\,|3\rangle$ with parameters $\theta, \phi \in [0, 2\pi]$ [33]. The accuracy of 93.660% is attainable by testing samples of this state over the non-toy model with the step-decay learning rate. In contrast, the testing accuracy of 98.000% is achieved for the toy model trained over $1,000$ toy samples of (27). Fig. 9 depicts the coherence prediction results for this toy detector.

C. Discord Classification

1) Dataset Formulation: The master dataset for discord includes a total of $80,000$ samples. This dataset comprises

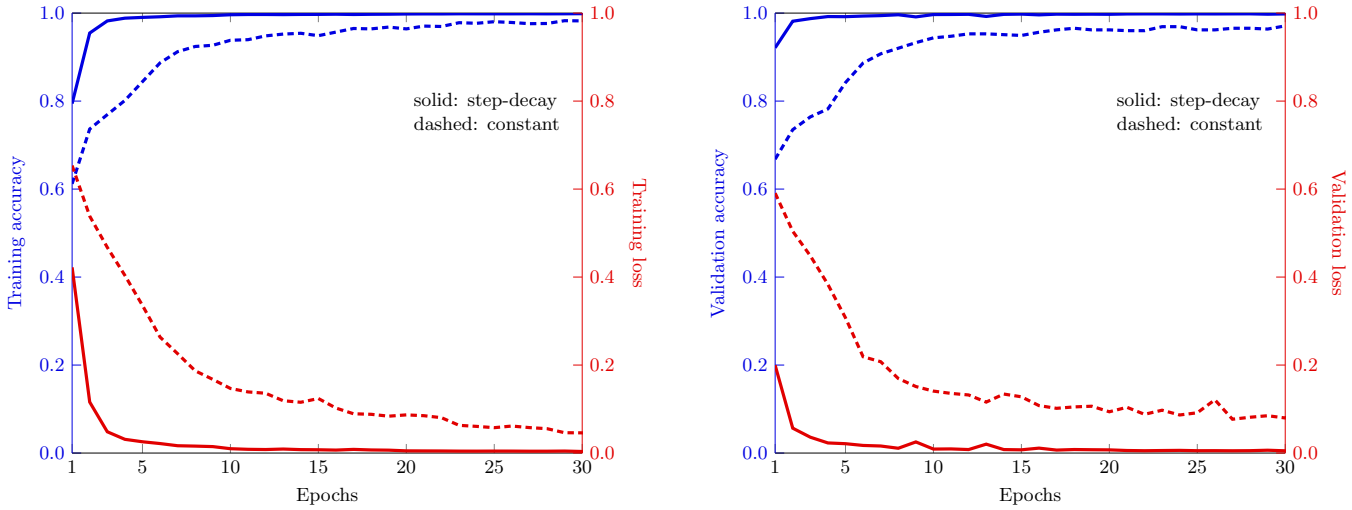

(a) Training (b) Validation

Fig. 12. Entanglement classification where (a) training and (b) validation accuracy and loss values are plotted as a function of epochs for the step-decay and constant learning rates.

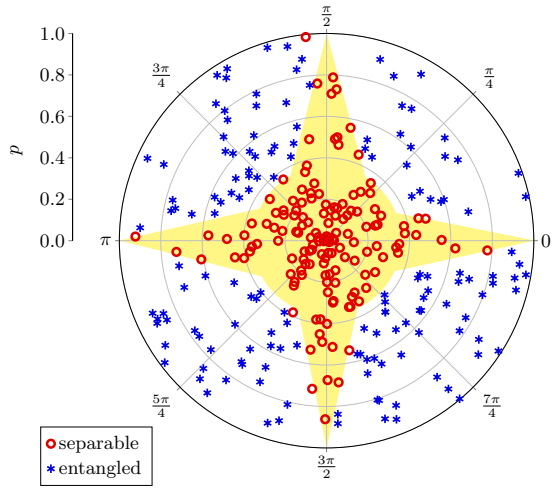

Fig. 13. Toy entanglement detection where the prediction results with the trained toy CNN model are depicted as a function of parameters (p, θ) for a toy example of (29) on entangled and unentangled regions. The blue and red data points represent predictions as entangled and unentangled, respectively. The yellow-shaded region depicts the actual unentangled region.

$20,000$ samples of RDMs with arbitrary rank r, $20,000$ samples of globally depolarized RDMs with arbitrary rank (r) and noise parameter (q) values, $20,000$ samples of product RDMs $(\boldsymbol{\rho}_{\rm A} \otimes \boldsymbol{\rho}_{\rm B})$, and $20,000$ samples of MDMSs.

2) Numerical Results: Fig. 10(a) shows the training results of the CNN model in quantum discord learning where the training accuracy quickly converges to 97.732% for the step-decay learning rate (initialized at 0.0001) and more slowly to 97.402% for the constant learning rate of $L_{\rm d} = 0.0001$. Similarly, the training loss converges to 6.363% for the step-decay learning rate and 7.570% for the constant learning rate. Fig. 10(b) validates the trained model where the validation accuracy and loss are 97.625% (96.654%) and 6.690% (9.609%) for the step-decay (constant) learning rate for new and unseen discordant or nondiscordant data instances. For this trained model, the testing accuracy and loss are 97.468% and 7.358% for the step-decay learning rate and 97.218% and 8.012% for the constant learning rate. Table I shows the classification reports for the trained LeNet-5 model.

3) Toy Discord Detection: The achievable quantum speed up for one-qubit DQC is signified by discord detection in the following state

$$\boldsymbol{\rho} = \frac{1}{4}\left(\boldsymbol{I}_{\rm A} \otimes \boldsymbol{I}_{\rm B} + p\boldsymbol{\sigma}_x \otimes \frac{\boldsymbol{U}_{\rm B} + \boldsymbol{U}_{\rm B}^{\dagger}}{2} + p\boldsymbol{\sigma}_y \otimes \frac{\boldsymbol{U}_{\rm B} - \boldsymbol{U}_{\rm B}^{\dagger}}{2\iota}\right) \tag{28}$$

where $\boldsymbol{\sigma}_x$ is the Pauli-x operator, $\boldsymbol{\sigma}_y$ is the Pauli-y operator, and $\boldsymbol{U}_{\rm B} = e^{\iota\theta}\boldsymbol{U}$ [83]. This state is discordant if $\boldsymbol{U}$ is Haar random unitary, while it is nondiscordant when $\boldsymbol{U}$ is Hermitian random unitary [84]. The non-toy discord detector exhibits the testing accuracy up to 82.666%, whereas the toy discord detector outperforms with 91% accuracy for the toy model trained over $5,000$ toy samples. Fig. 11 depicts the discord prediction results for this toy one-qubit DQC detectors. Herein, Haar random unitary operators are chosen for $p > 0.5$, while Hermitian random unitary operators are employed for $p < 0.5$.

D. Entanglement Classification

1) Dataset Formulation: The master dataset for entanglement includes $150,000$ total instances. This dataset comprises of $20,000$ samples for RDMs of each rank, $20,000$ samples of product RDMs, $20,000$ samples of globally depolarized pure RDMs ($r = 1$), and $10,000$ samples of depolarized RDMs for each $r = 2$, 3, and 4 with arbitrary noise parameter values q.

2) Numerical Results: Fig. 12(a) shows the training curves of the CNN model in quantum entanglement learning where the training accuracy and loss rapidly converge to 99.952% and 0.166%, respectively, using the step-decay learning rate (initialized at 0.001). On the other hand, with the constant

learning rate of $L_{\mathrm{e}} = 0.001$, the training accuracy and loss converge more slowly, reaching 99.710% and 0.735%, respectively. Fig. 12(b) validates the trained model where the validation accuracy and loss reach 99.825% (99.604%) and 0.512% (0.968%) for the step-decay (constant) learning rate, respectively. For this trained model, the testing accuracy and loss are 99.596% and 1.006% for the constant learning rate and 99.790% and 0.519% for the step-decay learning rate (see Table I for the classification reports).

3) Toy Entanglement Detection: For noisy teleportation, entanglement detection becomes relevant in Werner-like states:

$$\boldsymbol{\rho} = p\,|\mathsf{toy}_{\mathrm{e}}\rangle\langle\mathsf{toy}_{\mathrm{e}}| + \frac{(1-p)\,\boldsymbol{I}}{d} \tag{29}$$

where $|\mathsf{toy}_{\mathrm{e}}\rangle = \cos(\theta/2)\,|01\rangle + e^{\iota\phi}\sin(\theta/2)\,|10\rangle$ [85]. For predicting entanglement on the non-toy environment of the master dataset, the accuracy of 89.999% is achieved for the step-decay learning rate. However, using the toy dataset with $4,000$ training samples of (29), the model's accuracy improves to 99.333%. Fig. 13 depicts the entanglement prediction results for this toy detector.

IV. Conclusion

To devise a unified mechanism for fundamental QPL, we have put forth the UQWM framework, which employs *experiment-friendly* quantum witness measurements and *data-driven* ML to certify, quantify, and classify enigmatically linked fundamental quantum properties. Significantly low systematic and statistical errors in the numerical quantification of quantum properties indicate the mathematical rigorousness and noise robustness of this witness-based method. We have also established the relationship between supervised learning and quantum information engineering by utilizing CNNs to discern resourceful states from resourceless states. High accuracy and low loss levels indicate that the power of CNNs is unleashed in the reliable and unified detection of relevant quantum-resource states that signify their key role in the quantum information processing tasks. To sum up, this work not only motivates simultaneous characterization of fundamental quantum properties but also ushers efficient quantum state classification in cases where typical benchmarking techniques become inefficacious in quantum metrology, quantum communication, and quantum computation. In conclusion, there is significant potential for advancements in quantum state classification by integrating quantum information engineering and classical data-driven learning. One promising direction involves extending the UQWM framework to multipartite, multilevel quantum systems and device-independent scenarios for NISQ networking. Another promising approach is to utilize optimal Pauli basis descriptions and unsupervised learning techniques for more efficient classification of high-dimensional quantum systems. In addition, the witness-based QPL measures can be compared with established bonafide measures in the context of quantum state ordering and characterization within resource theories of fundamental quantum properties. Moreover, the development of multiclass classifiers for multilevel coherence, multipartite entanglement, and observer-dependent discord can further enhance the versatility of the UQWM framework, opening up new avenues for interdisciplinary research.

References

[1] M. Kliesch and I. Roth, "Theory of quantum system certification," *PRX Quantum*, vol. 2, no. 1, p. 010201, Jan. 2021.

[2] U. Khalid, J. ur Rehman, S. N. Paing, H. Jung, T. Q. Duong, and H. Shin, "Quantum network engineering in the NISQ age: Principles, missions, and challenges," *IEEE Netw.*, vol. 38, no. 1, pp. 112–123, Jan. 2024.

[3] J. ur Rehman, A. Farooq, and H. Shin, "Discrete Weyl channels with Markovian memory," *IEEE J. Sel. Areas Commun.*, vol. 38, no. 3, pp. 413–426, Mar. 2020.

[4] J. Eisert, D. Hangleiter, N. Walk, I. Roth, D. Markham, R. Parekh, U. Chabaud, and E. Kashefi, "Quantum certification and benchmarking," *Nat. Rev. Phys.*, vol. 2, no. 7, pp. 382–390, Jul. 2020.

[5] J. ur Rehman, S. Hong, Y.-S. Kim, and H. Shin, "Variational estimation of capacity bounds for quantum channels," *Phys. Rev. A*, vol. 105, no. 3, p. 032616, Mar. 2022.

[6] M. Cramer, M. B. Plenio, S. T. Flammia, R. Somma, D. Gross, S. D. Bartlett, O. Landon-Cardinal, D. Poulin, and Y.-K. Liu, "Efficient quantum state tomography," *Nat. Commun.*, vol. 1, no. 1, pp. 1–7, Dec. 2010.

[7] S. Ahmed, C. S. Muñoz, F. Nori, and A. F. Kockum, "Classification and reconstruction of optical quantum states with deep neural networks," *Phys. Rev. Research*, vol. 3, p. 033278, Sep. 2021.

[8] A. M. Palmieri, E. Kovlakov, F. Bianchi, D. Yudin, S. Straupe, J. D. Biamonte, and S. Kulik, "Experimental neural network enhanced quantum tomography," *npj Quantum Inf.*, vol. 6, no. 1, p. 20, Feb. 2020.

[9] S. Ghosh, A. Opala, M. Matuszewski, T. Paterek, and T. C. H. Liew, "Reconstructing quantum states with quantum reservoir networks," *IEEE Trans. Neural Netw. Learn. Syst.*, vol. 32, no. 7, pp. 3148–3155, Jul. 2021.

[10] H.-Y. Huang, R. Kueng, and J. Preskill, "Predicting many properties of a quantum system from very few measurements," *Nat. Phys.*, vol. 16, no. 10, pp. 1050–1057, Jun. 2020.

[11] G. Struchalin, Y. A. Zagorovskii, E. Kovlakov, S. Straupe, and S. Kulik, "Experimental estimation of quantum state properties from classical shadows," *PRX Quantum*, vol. 2, no. 1, p. 010307, Jan. 2021.

[12] B. Wu, J. Sun, Q. Huang, and X. Yuan, "Overlapped grouping measurement: A unified framework for measuring quantum states," *arXiv:2105.13091v1*, 2021.

[13] R. Horodecki, P. Horodecki, M. Horodecki, and K. Horodecki, "Quantum entanglement," *Rev. Mod. Phys.*, vol. 81, no. 2, p. 865, Jun. 2009.

[14] A. Streltsov, G. Adesso, and M. B. Plenio, "Colloquium: Quantum coherence as a resource," *Rev. Mod. Phys.*, vol. 89, no. 4, p. 041003, Oct. 2017.

[15] A. Bera, T. Das, D. Sadhukhan, S. S. Roy, A. S. De, and U. Sen, "Quantum discord and its allies: A review of recent progress," *Rep. Prog. Phys.*, vol. 81, no. 2, p. 024001, Dec. 2017.

[16] J. W. Z. Lau, K. H. Lim, H. Shrotriya, and L. C. Kwek, "NISQ computing: where are we and where do we go?" *AAPPS Bull.*, vol. 32, no. 1, p. 27, Sep. 2022.

[17] G.-L. Long, D. Pan, Y.-B. Sheng, Q. Xue, J. Lu, and L. Hanzo, "An evolutionary pathway for the quantum internet relying on secure classical repeaters," *IEEE Netw.*, vol. 36, no. 3, pp. 82–88, Jul. 2022.

[18] D. Pan, G.-L. Long, L. Yin, Y.-B. Sheng, D. Ruan, S. X. Ng, J. Lu, and L. Hanzo, "The evolution of quantum secure direct communication: On the road to the Qinternet," *IEEE Commun. Surveys Tuts.*, Feb. 2024 (Early Access), doi:10.1109/COMST.2024.3367535.

[19] C. Carmeli, T. Heinosaari, A. Karlsson, J. Schultz, and A. Toigo, "Verifying the quantumness of bipartite correlations," *Phys. Rev. Lett.*, vol. 116, no. 23, p. 230403, Jun. 2016.

[20] I. Šupić, J. Bowles, M.-O. Renou, A. Acín, and M. J. Hoban, "Quantum networks self-test all entangled states," *Nat. Phys.*, vol. 19, no. 5, pp. 670–675, May 2023.

[21] J. Helsen and S. Wehner, "A benchmarking procedure for quantum networks," *npj Quantum Inf.*, vol. 9, no. 1, p. 17, Feb. 2023.

[22] E. Chitambar and G. Gour, "Quantum resource theories," *Rev. Mod. Phys.*, vol. 91, no. 2, p. 025001, Apr. 2019.

[23] I. Marvian, R. W. Spekkens, and P. Zanardi, "Quantum speed limits, coherence, and asymmetry," *Phys. Rev. A*, vol. 93, no. 5, p. 052331, May 2016.

[24] D. Girolami, A. M. Souza, V. Giovannetti, T. Tufarelli, J. G. Filgueiras, R. S. Sarthour, D. O. Soares-Pinto, I. S. Oliveira, and G. Adesso, "Quantum discord determines the interferometric power of quantum states," *Phys. Rev. Lett.*, vol. 112, no. 21, p. 210401, May 2014.

[25] U. Khalid, J. ur Rehman, and H. Shin, "Metrologically resourceful multipartite entanglement under quantum many-body effects," *Quantum Sci. Technol.*, vol. 6, no. 2, p. 025007, Jan. 2021.

[26] J. Ma, Y. Zhou, X. Yuan, and X. Ma, "Operational interpretation of coherence in quantum key distribution," *Phys. Rev. A*, vol. 99, p. 062325, Jun. 2019.

[27] S. Pirandola, "Quantum discord as a resource for quantum cryptography," *Sci. Rep.*, vol. 4, no. 1, p. 6956, Nov. 2014.

[28] M. Epping, H. Kampermann, C. Macchiavello, and D. Bruß, "Multipartite entanglement can speed up quantum key distribution in networks," *New J. Phys.*, vol. 19, no. 9, p. 093012, Sep. 2017.

[29] Y. Huang, "Computing quantum discord is NP-complete," *New J. Phys.*, vol. 16, no. 3, p. 033027, Mar. 2014.

[30] R. Auccaise, J. Maziero, L. C. Céleri, D. O. Soares-Pinto, E. R. deAzevedo, T. J. Bonagamba, R. S. Sarthour, I. S. Oliveira, and R. M. Serra, "Experimentally witnessing the quantumness of correlations," *Phys. Rev. Lett.*, vol. 107, p. 070501, Aug. 2011.

[31] Y. Zhou, P. Zeng, and Z. Liu, "Single-copies estimation of entanglement negativity," *Phys. Rev. Lett.*, vol. 125, no. 20, p. 200502, Nov. 2020.

[32] F. G. S. L. Brandão, "Quantifying entanglement with witness operators," *Phys. Rev. A*, vol. 72, no. 2, p. 022310, Aug. 2005.

[33] M. Ringbauer, T. R. Bromley, M. Cianciaruso, L. Lami, W. S. Lau, G. Adesso, A. G. White, A. Fedrizzi, and M. Piani, "Certification and quantification of multilevel quantum coherence," *Phys. Rev. X*, vol. 8, no. 4, p. 041007, Oct. 2018.

[34] M. Zidan, A.-H. Abdel-Aty, D. M. Nguyen, A. S. Mohamed, Y. Al-Sbou, H. Eleuch, and M. Abdel-Aty, "A quantum algorithm based on entanglement measure for classifying Boolean multivariate function into novel hidden classes," *Results Phys.*, vol. 15, p. 102549, Dec. 2019.

[35] M. S. Abdalla, A. Obada, and M. Abdel-Aty, "Von-Neumann entropy and phase distribution of two mode parametric amplifier interacting with a single atom," *Ann. Phys.*, vol. 318, no. 2, pp. 266–285, Aug. 2005.

[36] M. Abdalla, M. Abdel-Aty, and A. Obada, "Quantum entropy of isotropic coupled oscillators interacting with a single atom," *Opt. Commun.*, vol. 211, no. 1, pp. 225–234, Oct. 2002.

[37] E. G. El-Hadidy, A. Farouk, M. Abdel-Aty, and S. Ghose, "Controlling steady-state entanglement and quantum discord through squeezing angle," *Chaos, Solit. Fractals*, vol. 128, pp. 382–389, Nov. 2019.

[38] W. Wang, J. Han, B. Yadin, Y. Ma, J. Ma, W. Cai, Y. Xu, L. Hu, H. Wang, Y. P. Song, M. Gu, and L. Sun, "Witnessing quantum resource conversion within deterministic quantum computation using one pure superconducting qubit," *Phys. Rev. Lett.*, vol. 123, no. 22, p. 220501, Nov. 2019.

[39] J. Ma, B. Yadin, B. Girolami, V. Vedral, and M. Gu, "Converting coherence to quantum correlations," *Phys. Rev. Lett.*, vol. 116, no. 16, p. 160407, Apr. 2016.

[40] J. M. Matera, D. Egloff, N. Killoran, and M. B. Plenio, "Coherent control of quantum systems as a resource theory," *Quantum Sci. Technol.*, vol. 1, no. 1, p. 01LT01, Aug. 2016.

[41] A. Streltsov, U. Singh, H. S. Dhar, M. N. Bera, and G. Adesso, "Measuring quantum coherence with entanglement," *Phys. Rev. Lett.*, vol. 115, p. 020403, Jul. 2015.

[42] Y. Yao, X. Xiao, L. Ge, and C. Sun, "Quantum coherence in multipartite systems," *Phys. Rev. A*, vol. 92, no. 2, p. 022112, Aug. 2015.

[43] N. H. Nguyen, E. C. Behrman, M. A. Moustafa, and J. E. Steck, "Benchmarking neural networks for quantum computations," *IEEE Trans. Neural Netw. Learn. Syst.*, vol. 31, no. 7, pp. 2522–2531, Jul. 2020.

[44] E. C. Behrman, R. E. F. Bonde, J. E. Steck, and J. F. Behrman, "On the correction of anomalous phase oscillation in entanglement witnesses using quantum neural networks," *IEEE Trans. Neural Netw. Learn. Syst.*, vol. 25, no. 9, pp. 1696–1703, Sept. 2014.

[45] S. Lu, S. Huang, K. Li, J. Li, J. Chen, D. Lu, Z. Ji, Y. Shen, D. Zhou, and B. Zeng, "Separability-entanglement classifier via machine learning," *Phys. Rev. A*, vol. 98, p. 012315, Jul. 2018.

[46] J. Roik, K. Bartkiewicz, A. Černoch, and K. Lemr, "Accuracy of entanglement detection via artificial neural networks and human-designed entanglement witnesses," *Phys. Rev. Applied*, vol. 15, p. 054006, May 2021.

[47] F. Zaman, A. Farooq, M. A. Ullah, H. Jung, H. Shin, and M. Z. Win, "Quantum machine intelligence for 6G URLLC," *IEEE Wireless Commun.*, vol. 30, no. 2, pp. 22–30, Apr. 2023.

[48] Y. Qian, X. Wang, Y. Du, X. Wu, and D. Tao, "The dilemma of quantum neural networks," *IEEE Trans. Neural Netw. Learn. Syst.*, Oct. 2022 (Early Access), doi:10.1109/TNNLS.2022.3208313.

[49] Y.-C. Ma and M.-H. Yung, "Transforming Bell's inequalities into state classifiers with machine learning," *npj Quantum Inf.*, vol. 4, no. 1, pp. 1–10, Jul. 2018.

[50] Y. Chen, Y. Pan, G. Zhang, and S. Cheng, "Detecting quantum entanglement with unsupervised learning," *Quantum Sci. Technol.*, vol. 7, no. 1, p. 015005, Nov. 2021.

[51] N. Asif, U. Khalid, A. Khan, T. Q. Duong, and H. Shin, "Entanglement detection with artificial neural networks," *Sci. Rep.*, vol. 13, no. 1, p. 1562, Jan. 2023.

[52] G. L. Giorgi and R. Zambrini, "Hallmarking quantum states: Unified framework for coherence and correlations," *Quantum*, vol. 2, p. 109, Dec. 2018.

[53] F. Shahandeh, M. J. Hall, and T. C. Ralph, "Measurement-device-independent approach to entanglement measures," *Phys. Rev. Lett.*, vol. 118, no. 15, p. 150505, Apr. 2017.

[54] C. Napoli, T. R. Bromley, M. Cianciaruso, M. Piani, N. Johnston, and G. Adesso, "Robustness of coherence: An operational and observable measure of quantum coherence," *Phys. Rev. Lett.*, vol. 116, no. 15, p. 150502, Apr. 2016.

[55] Y. Yuan, Z. Hou, J.-F. Tang, A. Streltsov, G.-Y. Xiang, C.-F. Li, and G.-C. Guo, "Direct estimation of quantum coherence by collective measurements," *npj Quantum Inf.*, vol. 6, no. 1, pp. 1–5, May 2020.

[56] Y.-T. Wang, J.-S. Tang, Z.-Y. Wei, S. Yu, Z.-J. Ke, X.-Y. Xu, C.-F. Li, and G.-C. Guo, "Directly measuring the degree of quantum coherence using interference fringes," *Phys. Rev. Lett.*, vol. 118, no. 2, p. 020403, Jan. 2017.

[57] N. Friis, G. Vitagliano, M. Malik, and M. Huber, "Entanglement certification from theory to experiment," *Nat. Rev. Phys.*, vol. 1, no. 1, pp. 72–87, Dec. 2019.

[58] W.-H. Zhang, C. Zhang, Z. Chen, X.-X. Peng, X.-Y. Xu, P. Yin, S. Yu, X.-J. Ye, Y.-J. Han, J.-S. Xu, G. Chen, C.-F. Li, and G.-C. Guo, "Experimental optimal verification of entangled states using local measurements," *Phys. Rev. Lett.*, vol. 125, p. 030506, Jul. 2020.

[59] J. Gao, L.-F. Qiao, Z.-Q. Jiao, Y.-C. Ma, C.-Q. Hu, R.-J. Ren, A.-L. Yang, H. Tang, M.-H. Yung, and X.-M. Jin, "Experimental machine learning of quantum states," *Phys. Rev. Lett.*, vol. 120, p. 240501, Jun. 2018.

[60] A. Dimić and B. Dakić, "Single-copy entanglement detection," *npj Quantum Inf.*, vol. 4, no. 1, pp. 1–8, Feb. 2018.

[61] O. Gühne, M. Reimpell, and R. F. Werner, "Estimating entanglement measures in experiments," *Phys. Rev. Lett.*, vol. 98, p. 110502, Mar. 2007.

[62] G. H. Aguilar, O. J. Farías, J. Maziero, R. M. Serra, P. H. S. Ribeiro, and S. P. Walborn, "Experimental estimate of a classicality witness via a single measurement," *Phys. Rev. Lett.*, vol. 108, p. 063601, Feb. 2012.

[63] J. Bae, D. Chruściński, and B. C. Hiesmayr, "Mirrored entanglement witnesses," *npj Quantum Inf.*, vol. 6, no. 1, pp. 1–7, Feb. 2020.

[64] R. A. Bertlmann and P. Krammer, "Bloch vectors for qudits," *J. Phys. A: Math. Theor.*, vol. 41, no. 23, p. 235303, May 2008.

[65] M. Paini, A. Kalev, D. Padilha, and B. Ruck, "Estimating expectation values using approximate quantum states," *Quantum*, vol. 5, p. 413, Mar. 2021.

[66] B. Dirkse, M. Pompili, R. Hanson, M. Walter, and S. Wehner, "Witnessing entanglement in experiments with correlated noise," *Quantum Sci. Technol.*, vol. 5, no. 3, p. 035007, Jun. 2020.

[67] S. T. Flammia and Y.-K. Liu, "Direct fidelity estimation from few Pauli measurements," *Phys. Rev. Lett.*, vol. 106, no. 23, p. 230501, Jun. 2011.

[68] G. Tóth and O. Gühne, "Detecting genuine multipartite entanglement with two local measurements," *Phys. Rev. Lett.*, vol. 94, p. 060501, Feb. 2005.

[69] D. Rosset, R. Ferretti-Schöbitz, J.-D. Bancal, N. Gisin, and Y.-C. Liang, "Imperfect measurement settings: Implications for quantum state tomography and entanglement witnesses," *Phys. Rev. A*, vol. 86, p. 062325, Dec. 2012.

[70] J. ur Rehman and H. Shin, "Entanglement-free parameter estimation of generalized Pauli channels," *Quantum*, vol. 5, p. 490, Jul. 2021.

[71] K. Y. Chew, N. M. Shah, and K. T. Chan, "Representation of SU(8) in Pauli basis," *arXiv:2003.09192v1*, 2020.

[72] K. Wang, Z. Song, X. Zhao, Z. Wang, and X. Wang, "Detecting and quantifying entanglement on near-term quantum devices," *npj Quantum Inf.*, vol. 8, no. 1, p. 52, May 2022.

[73] H. Ren, A. Lin, S. He, and X. Hu, "Quantitative coherence witness for finite dimensional states," *Ann. Phys.*, vol. 387, pp. 281–289, Oct. 2017.

[74] L. Knips, J. Dziewior, W. Kłobus, W. Laskowski, T. Paterek, P. J. Shadbolt, H. Weinfurter, and J. D. A. Meinecke, "Multipartite entanglement analysis from random correlations," *npj Quantum Inf.*, vol. 6, no. 1, p. 51, Jun. 2020.

[75] A. Streltsov, H. Kampermann, S. Wölk, M. Gessner, and D. Bruß, "Maximal coherence and the resource theory of purity," *New J. Phys.*, vol. 20, no. 5, p. 053058, May 2018.
[76] B. Jungnitsch, S. Niekamp, M. Kleinmann, O. Gühne, H. Lu, W.-B. Gao, Y.-A. Chen, Z.-B. Chen, and J.-W. Pan, "Increasing the statistical significance of entanglement detection in experiments," *Phys. Rev. Lett.*, vol. 104, p. 210401, May 2010.
[77] U. Singh, M. N. Bera, H. S. Dhar, and A. K. Pati, "Maximally coherent mixed states: Complementarity between maximal coherence and mixedness," *Phys. Rev. A*, vol. 91, p. 052115, May 2015.
[78] F. Galve, G. L. Giorgi, and R. Zambrini, "Maximally discordant mixed states of two qubits," *Phys. Rev. A*, vol. 83, p. 012102, Jan. 2011.
[79] B.-H. Wang, "Entangled states in the role of witnesses," *Phys. Rev. A*, vol. 97, no. 5, p. 050302, May 2018.
[80] S. Kumar, "Wishart and random density matrices: Analytical results for the mean-square Hilbert-Schmidt distance," *Phys. Rev. A*, vol. 102, no. 1, p. 012405, Jul. 2020.
[81] C. Harney, M. Paternostro, and S. Pirandola, "Mixed state entanglement classification using artificial neural networks," *New J. Phys.*, vol. 23, no. 6, p. 063033, Jun. 2021.
[82] D. Girolami, T. Tufarelli, and G. Adesso, "Characterizing nonclassical correlations via local quantum uncertainty," *Phys. Rev. Lett.*, vol. 110, p. 240402, Jun. 2013.
[83] B. Dakić, V. Vedral, and Č. Brukner, "Necessary and sufficient condition for nonzero quantum discord," *Phys. Rev. Lett.*, vol. 105, p. 190502, Nov. 2010.
[84] U. Khalid, J. ur Rehman, and H. Shin, "Measurement-based quantum correlations for quantum information processing," *Sci. Rep.*, vol. 10, p. 2443, Feb. 2020.
[85] N. Ganguly, S. Adhikari, A. Majumdar, and J. Chatterjee, "Entanglement witness operator for quantum teleportation," *Phys. Rev. Lett.*, vol. 107, no. 27, p. 270501, Dec. 2011.

Uman Khalid received his B.S. degree in electronics engineering from the Ghulam Ishaq Khan (GIK) Institute, Topi, Pakistan, in 2015 and his Ph.D. in electronics engineering from Kyung Hee University, South Korea, in Feb. 2023. Since Mar. 2023, he has been a Post-Doctoral Fellow with the Department of Electronics and Information Convergence Engineering, Kyung Hee University. His research interests include quantum information science, quantum metrology, and quantum networks.

Junaid ur Rehman received the B.S. degree in Electrical Engineering from National University of Sciences and Technology (NUST), Islamabad, Pakistan, in 2013, and the Ph.D. degree in Electronic Engineering from Kyung Hee University (KHU), Yongin-si, Korea, in 2019.

He worked as a Postdoctoral Fellow at KHU (2019-2020) and Korea Institute of Science and Technology (KIST) (2020). Later he joined KHU as a Research Professor from 2021-2022. In 2022, he joined the Interdisciplinary Centre for Security, Reliability and Trust (SnT), University of Luxembourg where he is currently a Research Scientist in the Signal Processing and Communications (SigCom) group. His research interests include quantum information sciences that include quantum communications, quantum computing, and quantum sensing.

Dr. ur Rehman has served as a technical program committee member of multiple IEEE conferences including IEEE International Conference on Communications (ICC) and IEEE Global Communications Conference (Globecom). He has reviewed for numerous IEEE conferences and journals. He was an Exemplary Reviewer for the IEEE WIRELESS COMMUNICATIONS LETTERS in 2022.

Haejoon Jung (Senior Member, IEEE) received the B.S. degree (Hons.) in electrical engineering from Yonsei University, Seoul, South Korea, in 2008, and the M.S. and Ph.D. degrees in electrical engineering from the Georgia Institute of Technology (Georgia Tech), Atlanta, GA, USA, in 2010 and 2014, respectively. From 2014 to 2016, he was a Wireless Systems Engineer at Apple, Cupertino, CA, USA. From 2016 to 2021, he was with Incheon National University, Incheon, South Korea. Since September 2021, he has been with the Department of Electronic Engineering, Kyung Hee University, as an Associate Professor. His research interests include communication theory, wireless communications, wireless power transfer, and statistical signal processing. He was a recipient of the Haedong Young Scholar Award from the Korean Institute of Communications and Information Sciences. He serves as an Editor for IEEE TRANSACTIONS ON COMMUNICATIONS, IEEE TRANSACTIONS ON VEHICULAR TECHNOLOGY, IEEE TRANSACTIONS ON AEROSPACE AND ELECTRONIC SYSTEMS, IEEE COMMUNICATIONS LETTERS, IEEE WIRELESS COMMUNICATIONS LETTERS, and ICT EXPRESS.

Trung Q. Duong (Fellow, IEEE) is a Canada Excellence Research Chair (CERC) and a Full Professor at Memorial University, Canada. He is also the adjunct Chair Professor in Telecommunications at Queen's University Belfast, UK and a Research Chair of Royal Academy of Engineering, UK. He was a Distinguished Advisory Professor at Inje University, South Korea (2017-2019), an Adjunct Professor and the Director of Institute for AI and Big Data at Duy Tan University, Vietnam (2012-present), and a Visiting Professor (under Eminent Scholar program) at Kyung Hee University, South Korea (2023-2025). His current research interests include quantum communications, wireless communications, quantum machine learning, and optimisation.

Dr. Duong has served as an Editor/Guest Editor for the IEEE TRANSACTIONS ON WIRELESS COMMUNICATIONS, IEEE TRANSACTIONS ON COMMUNICATIONS, IEEE TRANSACTIONS ON VEHICULAR TECHNOLOGY, IEEE COMMUNICATIONS LETTERS, IEEE WIRELESS COMMUNICATIONS LETTERS, IEEE WIRELESS COMMUNICATIONS, IEEE COMMUNICATIONS MAGAZINES, and IEEE JOURNAL ON SELECTED AREAS IN COMMUNICATIONS. He received the Best Paper Award at the IEEE VTC-Spring 2013, IEEE ICC 2014, IEEE GLOBECOM 2016, 2019, 2022, IEEE DSP 2017, IWCMC 2019, 2023, and IEEE CAMAD 2023. He has received the two prestigious awards from the Royal Academy of Engineering (RAEng): RAEng Research Chair (2021-2025) and the RAEng Research Fellow (2015-2020). He is the recipient of the prestigious Newton Prize 2017.

Octavia A. Dobre (Fellow, IEEE) is a Professor and Tier-1 Canada Research Chair with Memorial University, Canada. She was a Visiting Professor with Massachusetts Institute of Technology, USA and Université de Bretagne Occidentale, France.

Her research interests encompass wireless communication and networking technologies, as well as optical and underwater communications. She has (co-)authored over 500 refereed papers in these areas.

Dr. Dobre serves as the VP Publications of the IEEE Communications Society. She was the inaugural Editor-in-Chief (EiC) of the IEEE OPEN JOURNAL OF THE COMMUNICATIONS SOCIETY and the EiC of the IEEE COMMUNICATIONS LETTERS.

Dr. Dobre was a Fulbright Scholar, Royal Society Scholar, and Distinguished Lecturer of the IEEE Communications Society. She obtained 7 IEEE Best Paper Awards including the 2024 Heinrich Hertz Award. Dr. Dobre is an elected member of the European Academy of Sciences and Arts, a Fellow of the Engineering Institute of Canada, and a Fellow of the Canadian Academy of Engineering.

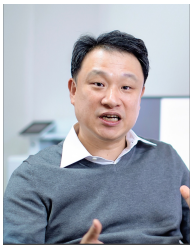

Hyundong Shin (Fellow, IEEE) received the B.S. degree in Electronics Engineering from Kyung Hee University (KHU), Yongin-si, Korea, in 1999, and the M.S. and Ph.D. degrees in Electrical Engineering from Seoul National University, Seoul, Korea, in 2001 and 2004, respectively. During his post-doctoral research at the Massachusetts Institute of Technology (MIT) from 2004 to 2006, he was with the Laboratory for Information Decision Systems (LIDS). In 2006, he joined the KHU, where he is currently a Professor in the Department of Electronic Engineering. His research interests include quantum information science, wireless communication, and machine intelligence. Dr. Shin received the IEEE Communications Society's Guglielmo Marconi Prize Paper Award and William R. Bennett Prize Paper Award. He served as the Publicity Co-Chair for the IEEE PIMRC and the Technical Program Co-Chair for the IEEE WCNC and the IEEE GLOBECOM. He was an Editor of IEEE TRANSACTIONS ON WIRELESS COMMUNICATIONS and IEEE COMMUNICATIONS LETTERS.